ELECTRICAL CONDUCTION IN NIOBIUM SELENIDE

by

Jack Spencer Edwards

B.A. (Honours), Cambridge University, 1966

A THESIS SUBMITTED IN PARTIAL FULFILMENT OF
THE REQUIREMENTS FOR THE DEGREE OF
MASTER OF SCIENCE

in the Department

of

Physics

SIMON FRASER UNIVERSITY

August 1971

APPROVAL

Name : Jack Spencer Edwards

Degree : Master of Science

Title of Thesis : Electrical conduction in niobium selenide

Examining Committee :

Chairman : Dr. K.E. Rieckhoff

Dr. R.F. Frindt
Senior Supervisor

Dr. D.J. Huntley

Dr. S. Gygax

Dr. E.J. Wells

Associate Professor
Department of Chemistry, Simon Fraser University

Date approved : Aug 9, 1971.

ABSTRACT

The metallic layer structure niobium selenide ($NbSe_2$) was synthesized from its elements, and single crystals prepared by using iodine vapour transport. The use of lower temperature gradients and longer transport times than in previous work on $NbSe_2$ resulted in the formation of larger crystals. New experiments are now possible with these larger samples.

The resistivity of $NbSe_2$ was measured across the layers ($\parallel$ c) by a four probe technique that could be used for other layer structures. The temperature dependent part of the resistivity $\rho_{\parallel c}$ was found to be linear in T from 300°K to 80°K and had a T^3 dependence below 60°K. The ratio of the resistivities $\rho_{\parallel c}/\rho_{\perp c}$ was constant at 31 : 1 from 300°K to 80°K and then fell linearly with temperature.

Single crystal nuclear magnetic resonance studies were made at 77°K and 17°K and indicate the presence of two conduction bands. A Hall coefficient sign reversal has been observed by other workers at 26°K. Some possible explanations of this are discussed in relation to the results of resistivity, Hall effect and nuclear magnetic resonance experiments.

Acknowledgements

I am grateful to Dr. R.F. Frindt for suggesting the research topic, and for his encouragement and advice throughout the entire research period. Dr. D.J. Huntley contributed greatly, especially with regard to the discussion of the two-band model presented in chapter 5.

I acknowledge the facilities for broad-line NMR measurements that were made available to me by Dr. D.L. Williams at the University of British Columbia, and for the expert assistance of Mr. J. Schratter and Dr. J. Trodahl in the carrying out of the experiments. Dr. E.J. Wells read through chapter 4 and the final version was improved by his helpful remarks.

I thank Mr. Wayne Sievers for most of the draughting and Margaret Bennett for the typing of the manuscript.

The financial assistance of the President's Research Grant and of the National Research Council of Canada is gratefully acknowledged.

Table of Contents

List of tables

List of figures

Chapter 1 : Introduction

1.1 Transition metal dichalcogenides

The transition metals of groups IV - VII of the periodic table combine with the chalcogens (S, Se, Te) to form layered dichalcogenides of the form MX_2 where M = metal and X = chalcogen. Within the X - M - X layer the atoms are held together strongly by covalent bonds, but each layer is only bound weakly to the next layer. The interlayer binding forces are thought to be of the van der Waals type. Figure 1.1 shows the general form (in section) of these layer structures. The co-ordination unit for the MX_2 layer structures may be either trigonal prismatic (molybdenite structure) or octahedral (cadmium iodide structure). Both are shown in figure 1.2. The unit cell is formed from 2,3,4 or 6 layers, depending on the particular material and the method of preparation. Hulliger (1968) and Wilson and Yoffe (1969) have published full reviews and details of the crystallography may be found there.

Structurally and chemically the MX_2 materials form a well-defined family, but their electronic properties show wide variations. For example, HfS_2 is an insulator, MoS_2 and WSe_2 are semiconducting, while NbS_2 and $NbSe_2$ are metals. Optical studies (Wilson and Yoffe 1969) have led to the adoption of tentative band models, but these are not yet sufficiently detailed for accurate calculations to be made of electric and

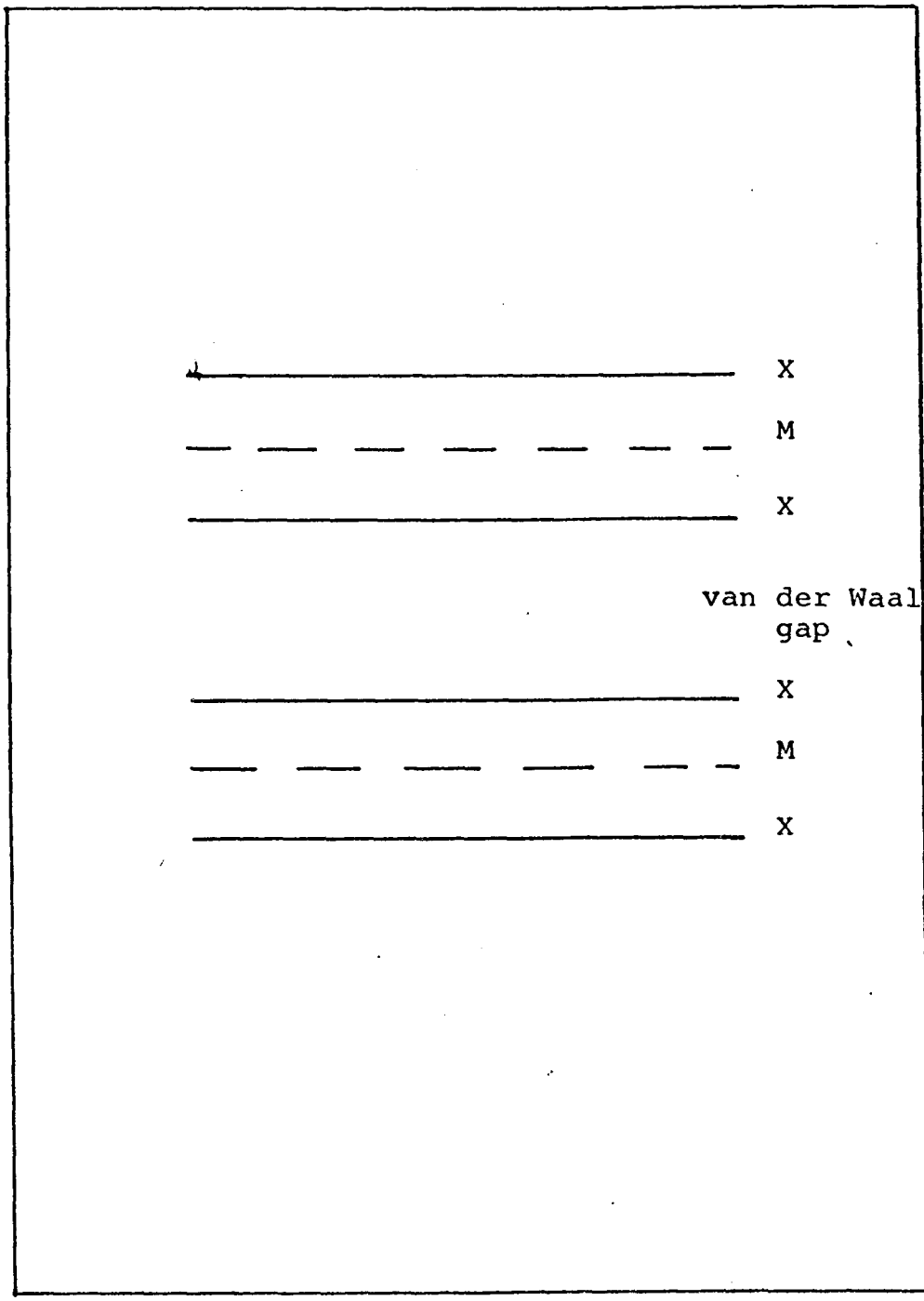

Fig. 1.1 Arrangement of successive sheets in the MX_2 layered transition metal dichalcogenides.

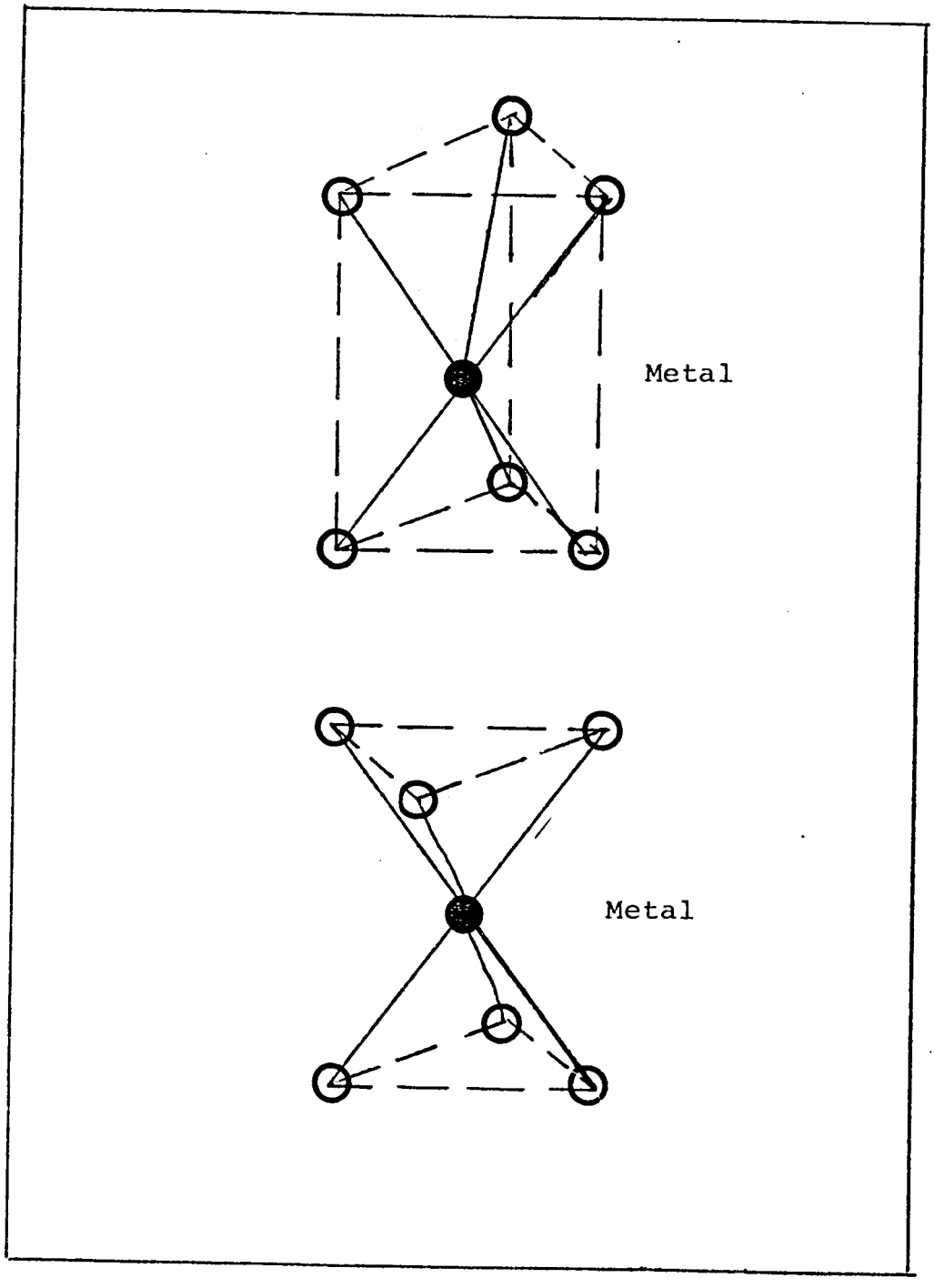

Fig. 1.2 Co-ordination units for MX_2 layer structures. Trigonal prismatic (molybdenite) structure is shown above and cadmium iodide (octahedral) is shown below .

magnetic properties.

The basic atomic structure of loosely connected layers makes such materials extremely anisotropic in many of their physical properties. In this respect there is a similarity between the MX_2 layer structures and graphite.

Measurement of the anisotropies in physical properties requires the use of single crystals, which, with the exception of molybdenite (MoS_2), have to be prepared artificially. They are first prepared as fine powders by synthesis from stoichiometric proportions of their elements, and the single crystals are made by chemical vapour transport, using bromine or iodine as the carrier. (Brixner 1962, Schafer 1964)

1.2 Previous work on $NbSe_2$

$NbSe_2$ exists in two forms, one with two layers to the unit cell (Brixner 1962) and one with four (Revolinsky 1965). The two layer (2H) modification is formed at 850°C or lower in the reaction tube, while the four layer modification (4H) is formed at 900°C or higher. Iodine transport at temperatures of 800°C or lower ensures that only the 2H single crystals form at the cool end of the reaction tube. The two stacking polytypes are both superconducting, the 2H having a transition temperature of 7.0°K and the 4H having one of 6.3°K (Revolinsky 1965). Little work has been done on the 4H stacking polytype,

and this thesis will concern itself exclusively with the 2H modification. Structurally, the 2H - $NbSe_2$ has the molybdenite structure as shown in figure 1.3.

Lee (1969) has measured the resistivity and Hall coefficient for currents perpendicular to the c-axis of the single crystal. The resistivity shows no remarkable features, but the Hall coefficient (Fig. 1.4) shows an abrupt change of sign at 26°K, being p-type at $T \geq 26^{\circ}K$ and n-type at $T \leq 26^{\circ}K$. This change is reminiscent of a phase change and various explanations have been offered (Lee 1970, Geballe 1971). Magnetic susceptibility measurements have been made (Selte 1965, Lee 1970), and from these it was concluded that $NbSe_2$ was antiferromagnetic below about 50°K. However, the presence of iron impurities in the samples used makes this conclusion of doubtful validity (Wold 1971). No changes in the crystallographic parameters have been observed (Lee 1970, Geballe 1971) but from his NMR observations on powders Geballe (1971) suggests that there may be an electronic rearrangement of orbitals below 26°K.

Optical studies (Wilson and Yoffe 1969) show absorption band edges in the visible and near infra-red. Both Wilson and Yoffe (1969) and Goodenough (1968) have published band schemes for $NbSe_2$. They are characterised by narrow d-bands with energy near the Fermi energy. The d_{Z2} band is half-full, giving $NbSe_2$ its metallic character. Far infra-red spectra (Clayman 1971) show that the superconducting energy gap

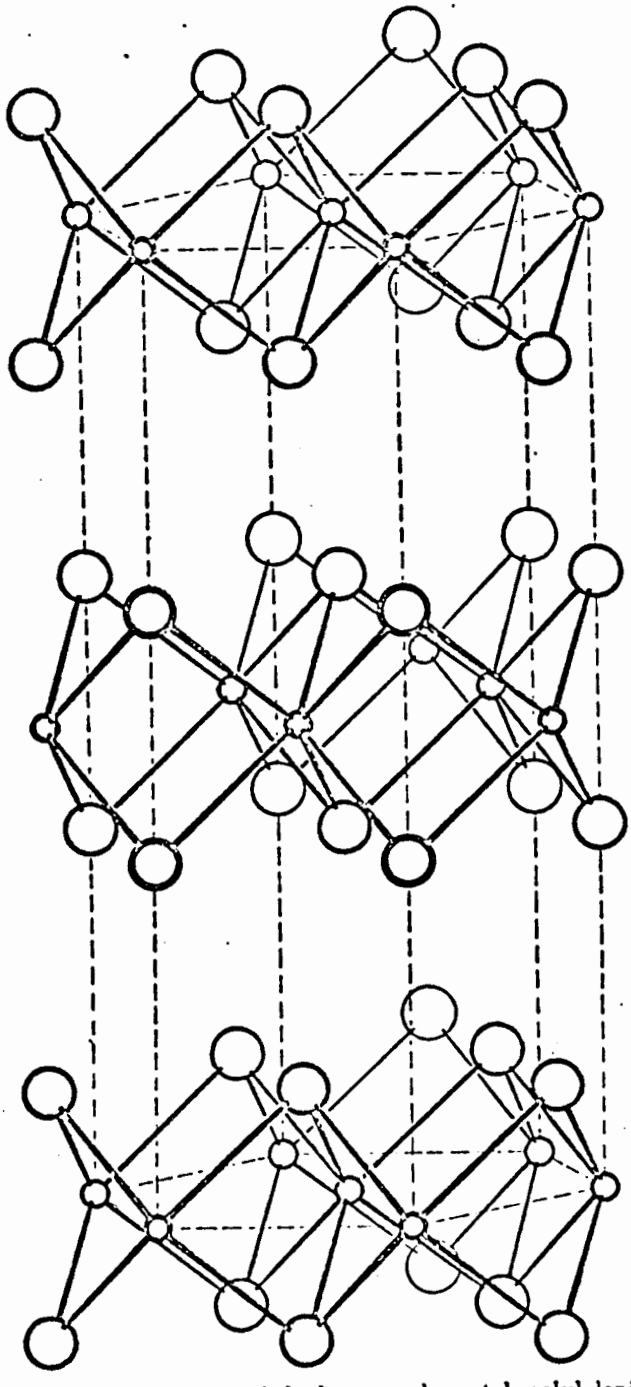

FIG. 15–6.—The structure of the hexagonal crystal molybdenite, MoS_2, showing the arrangement of sulfur atoms (large circles) at the corners of a trigonal prism about each molybdenum atom (small circles).

Fig. 1.3 Structure of 2H- MoS_2 (after Pauling) . $NbSe_2$ has an almost identical structure, with only a slight difference in stacking order.

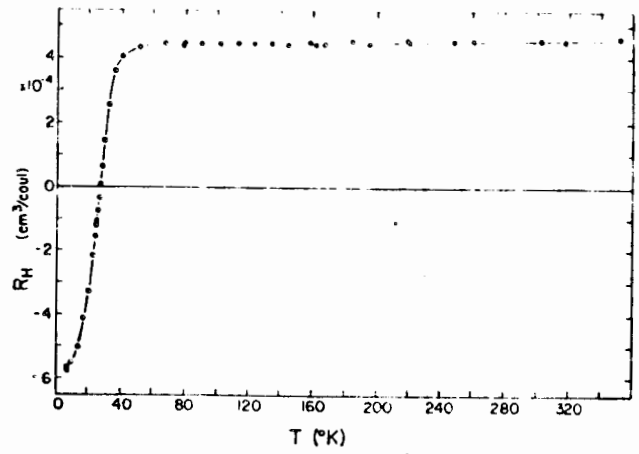

Fig. 1.4 Plot of the Hall coefficient of $NbSe_2$ as a function of temperature . (after Lee (1969))

depends on temperature in the way required by the B.C.S. theory (Bardeen 1957).

1.3 Contributions of this thesis

There are three experimental chapters in this thesis, each dealing with one aspect of the problem of electrical conduction in $NbSe_2$.

Chapter 2 describes a method of growing larger single crystals so that previously impossible experiments such as single crystal NMR or off-edge reflectivity are now feasible.

Chapter 3 describes a direct method of determining the anisotropy in the electrical resistivity of $NbSe_2$. The method could, in principle, be applied to any of the MX_2 layer structures.

Chapter 4 describes the single crystal NMR measurements that were made to explore the nature of the changes that resulted in the Hall coefficient changing sign.

The discussion in chapter 5 examines the various hypotheses put forward to explain the resistivity of $NbSe_2$ in the light of the experimental evidence.

Chapter 2 : Preparation of single crystals of niobium selenide

2.1 Materials used

The niobium selenide used for all the experiments was prepared by synthesis from the elements. Single crystals were made by the use of chemical vapour transport, using iodine as the carrier. The 99.93% niobium and the 99.999% selenium were obtained from United Mineral and Chemical Corp., New York and the analysis report showed that the major impurities were iron, silicon and tantalum*. Tantalum is so similar chemically to niobium that it would not be expected to affect the properties of niobium selenide too much, but small concentrations of iron in metals result in drastic changes in their electric and magnetic properties at low temperatures (Borelius 1932, Kopp 1969).

2.2 Preparation of the single crystals

The general method follows that used by Kershaw et al (Kershaw 1965). Stoichiometric proportions of niobium and

---

*Impurity levels in the niobium (parts per million by weight)
Iron 200 Silicon 200 Tantalum 100 Sodium 5 Manganese 1
These are taken from spectrographic analysis performed by supplier. Impurity levels in the selenium are negligible by comparison.

selenium were placed in a clean quartz reaction tube, which was then evacuated to a pressure of 10^{-5} - 10^{-6} torr. The tube was then sealed and placed in a Lindberg single-zone furnace at 650°C for 100 hours. A fine powder of niobium selenide was formed as a result.

To prepare the single crystals about 5gm of the $NbSe_2$ powder was placed in a quartz transport tube about 35cm long and the tube was pumped to 10^{-6} torr. Iodine was weighed out so as to give a concentration of 5 mg/cm^3 in the transport tube. It was then placed in a glass ampoule and pumped to 10^{-1} torr at 0°C. This ensured that all the water vapour was pumped away, while the iodine remained solid. The sealed ampoule was then placed in the vacuum system, broken, and the iodine sublimed into the transport tube. Figure 2.1 shows the experimental arrangement used for the iodine sublimation. The transport tube was cooled to 77°K to make the process more efficient.

The transport tube was then sealed and placed in a Lindberg three-zone furnace for iodine transport. The furnace was set at 850°C for 50 hours with one end plug out in order to clean the tube by back transport. The main transport reaction took place at 750°C (charge zone) and 725°C (growth zone) for 200 hours with both end plugs in, with a further 50 hours at 700°C (charge) and 675°C (growth) to ensure maximum transport.

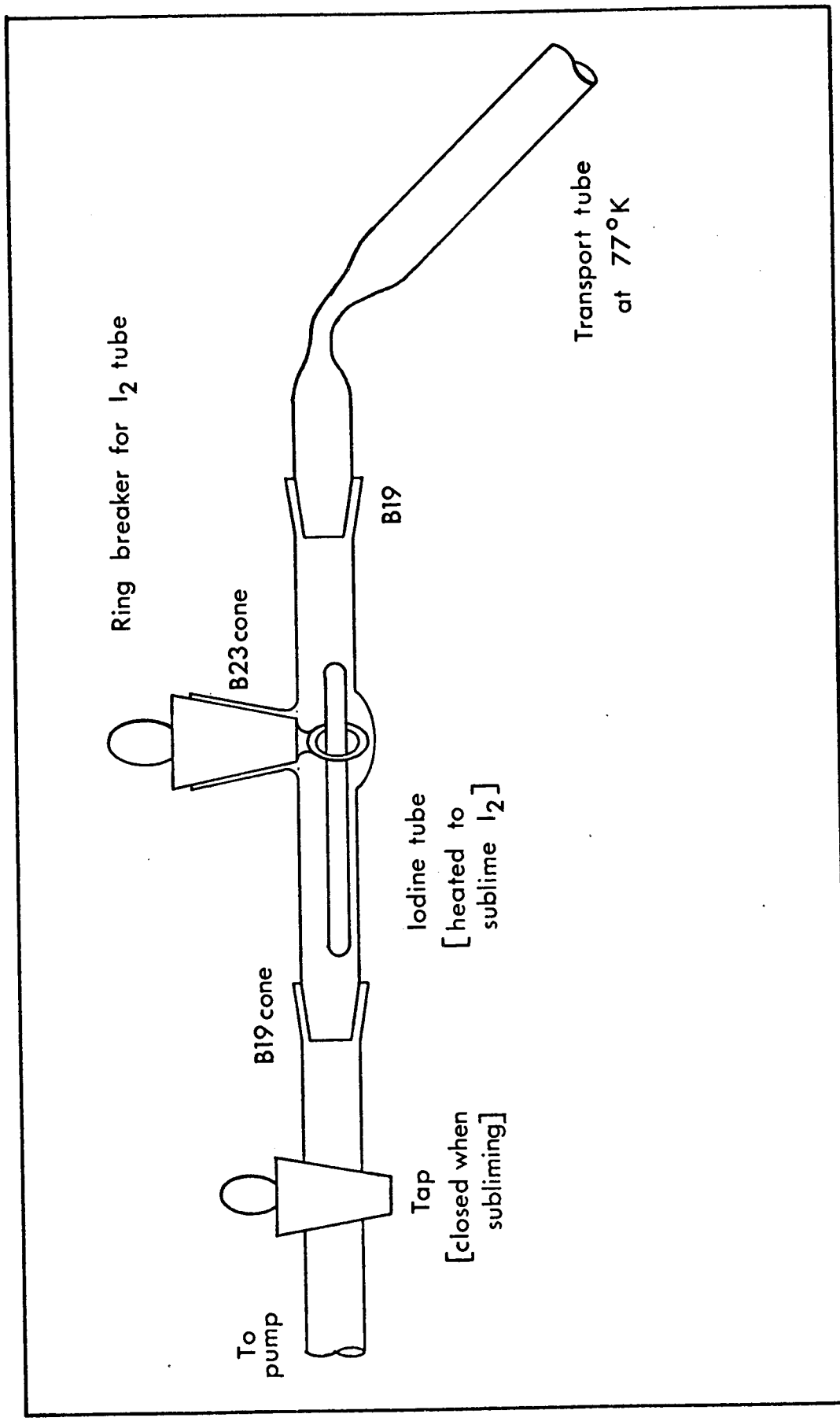

Fig. 2.1 Iodine sublimation arrangement used in the chemical vapour transport.

A temperature profile of the three-zone furnace, measured with a standard chromel-alumel thermocouple is shown in figure 2.2.

The resulting crystals were of the form of thin platelets of all sizes up to 2cm x 2cm x 0.1cm. They had shiny surfaces and appeared free from major defects, although some of the larger ones had clear growth spirals on the faces perpendicular to the c-axis. The crystals were washed in acetone to wash off surplus iodine and stored in a dessicator to keep them dry and free from dust.

No detailed chemical analysis of the crystals was undertaken, but the superconducting transition temperature was measured to be 7.0°K. This showed that there was none of the four-layer modification of $NbSe_2$ present (transition temperature 6.3°K, Revolinsky 1965) and also that any departures from stoichiometry were small, since the transition temperature is very sensitive to minor variations in the niobium concentration (Antonova 1969). Other workers (Kershaw 1965) have shown that the iodine concentration in the crystals is less than 1 part in 10^5.

2.3 Chemistry of the transport reaction

The general theory of vapour transport reactions is dealt with by Schafer (1964) and its application to the

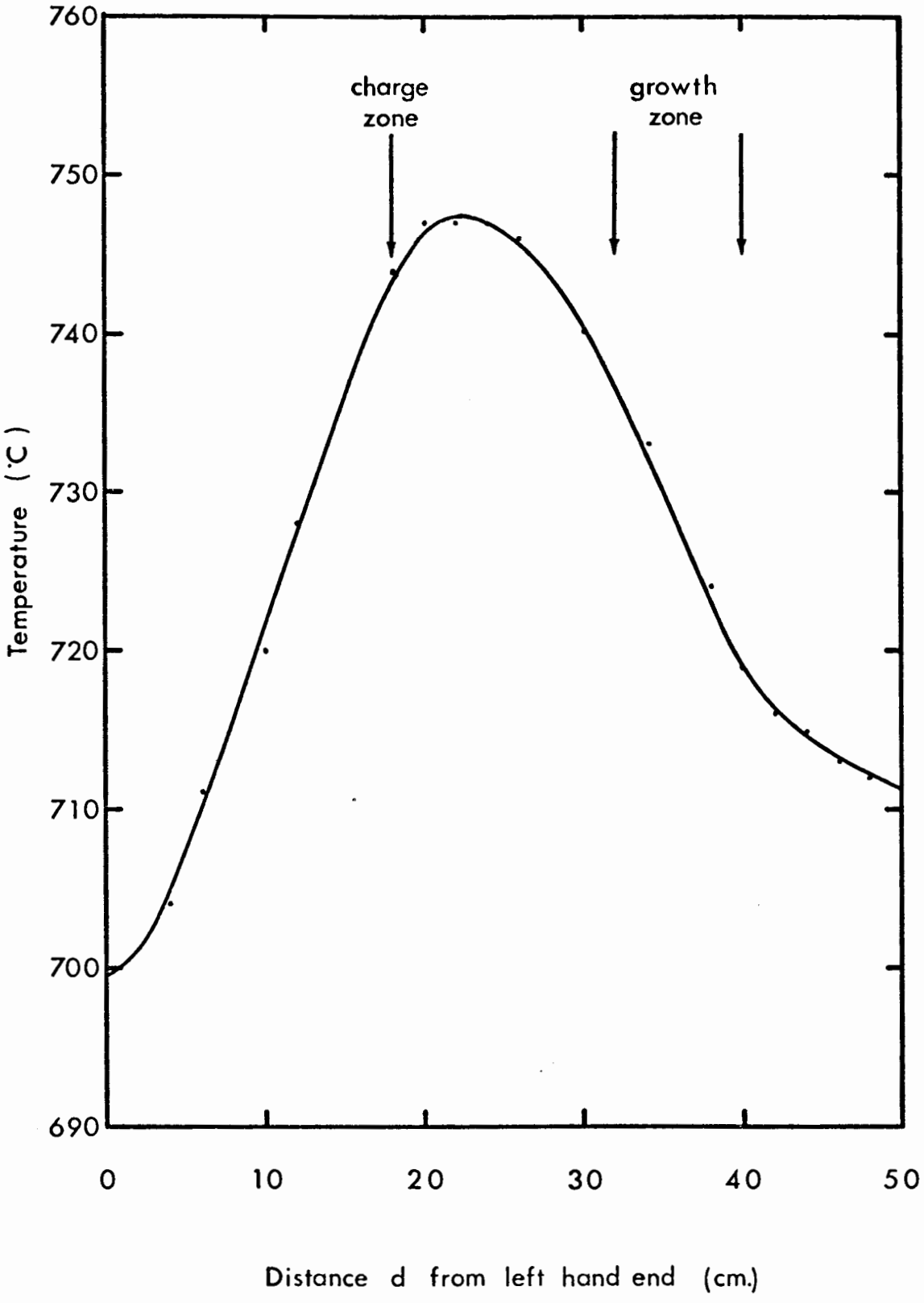

Fig. 2.2 Temperature profile of the three-zone furnace used for iodine vapour transport of $NbSe_2$ powder .

niobium-selenium system by Brixner (1962).

At the hot end of the tube the niobium selenide is converted to iodide in accordance with the following reaction:

$$2NbSe_{2(s)} + 5I_{2(g)} \rightleftharpoons 2NbI_{5(s)} + 4Se_{(g)} \qquad (2\text{-}1)$$

The gaseous products proceed by diffusion and thermal convection to the cool end of the tube where niobium selenide is re-formed, this time as a single crystal.

$$2NbI_{5(g)} + 4Se_{(g)} \rightleftharpoons 2NbSe_{2(s)} + 5I_{2(g)} \qquad (2\text{-}2)$$

The iodine diffuses back to transport more niobium selenide.

In the earlier work (Brixner 1962, Kershaw 1965) the temperature difference between the hot and cold ends of the tube was of the order of 200°C and the transport was complete in 10 - 15 hours. The smaller temperature gradients emplcyed in this work meant that the reactions took longer because of the slower movements of the gases within the tube (Schafer 1964, pp. 31-32). However, larger crystals result from the slower process. This is exactly analagous to the slow growth processes of other large single crystals from solutions and melts.

Of the three major impurities present in the Nb used,

silicon is not transported as the silicon-iodine reaction is not reversible. One of the preconditions for vapour transport is that all the reactions should be reversible (Schafer 1964, pp. 31-32).

Tantalum is transported as the preparation of single crystals of tantalum selenide is almost exactly the same as that for niobium selenide. It was not clear at the outset whether iron would be transported so a run was made with pure iron selenide under exactly the same conditions of temperature, time and vacuum as was a niobium selenide run. It was found that iron selenide formed flat crystals at the cool end of the tube. It can therefore be presumed that the major impurities in the niobium selenide single crystals are iron and tantalum, both with concentrations of the order of 100 molecular parts per million (i.e. 100 atoms of iron or tantalum per million molecules of niobium selenide). X-ray diffraction studies can determine the form of the iron impurity if the $NbSe_2$ is doped with 1% iron. From consideration of atomic sizes the Fe atom (diam. 1.48 Å) can either replace the Nb atom (diam. 2.00 Å) substitutionally or occupy a position between the layers (width of gap 3.59 Å, Brown 1965). The iron impurity concentration of 100 ppm is too low for the X-ray measurements to be conclusive with the as-grown crystals.

Chapter 3 : Resistivity measurements on $NbSe_2$

3.1 Electrical conductivity in anisotropic media

In a homogenous, isotropic conductor the electric current density $\underline{J}$ is related to the electric field intensity $\underline{E}$ by:

$$\underline{J} = \sigma \underline{E} \tag{3-1}$$

where σ is the conductivity. In this case $\underline{J}$ and $\underline{E}$ are in the same direction and σ is a scalar.

When Eq. (3-1) is generalised for the case of anisotropic media $\underline{J}$ and $\underline{E}$ are not necessarily in the same direction and now $\underline{\underline{\sigma}}$ is a second rank tensor.

$$\underline{J} = \underline{\underline{\sigma}} \cdot \underline{E} \tag{3-2}$$

The conductivity tensor $\underline{\underline{\sigma}}$ will have nine components but not all will be independent of one another. The tensor must have the same symmetry transformations as the crystal (Nye 1957, ch. 1) and this reduces the number of independent components. Referred to its principal axis:

$$\underline{\underline{\sigma}} = \begin{pmatrix} \sigma_{11} & 0 & 0 \\ 0 & \sigma_{22} & 0 \\ 0 & 0 & \sigma_{33} \end{pmatrix} \tag{3-3}$$

One of these principal axes is the c-axis in the case of niobium selenide, and there is a 6-fold rotational symmetry about this axis (Brown 1965). No special axis is defined in the plane perpendicular to c, so by symmetry $\sigma_{11} = \sigma_{22}$. Thus the nine components have been reduced to two: σ_{11} the conductivity perpendicular to c and σ_{33}, the conductivity parallel to c.

The quantity to be measured resistivity $\underline{\underline{\rho}}$, is the inverse of the conductivity. Thus,

$$\underline{\underline{\rho}} \cdot \underline{\underline{\sigma}} = \underline{\underline{1}} \qquad (3\text{-}4)$$

The same symmetry considerations that applied to the conductivity also apply to the resistivity, so the resistivity tensor is of exactly the same form, having just two independent components. They are defined as $\rho_{\parallel c}$, the resistivity parallel to c and $\rho_{\perp c}$ the resistivity perpendicular to c. Substituting into Eq. (3-4):

$$\begin{pmatrix} \rho_{\perp c} & 0 & 0 \\ 0 & \rho_{\perp c} & 0 \\ 0 & 0 & \rho_{\parallel c} \end{pmatrix} \cdot \begin{pmatrix} \sigma_{11} & 0 & 0 \\ 0 & \sigma_{11} & 0 \\ 0 & 0 & \sigma_{33} \end{pmatrix} = \begin{pmatrix} 1 & 0 & 0 \\ 0 & 1 & 0 \\ 0 & 0 & 1 \end{pmatrix} \qquad (3\text{-}5)$$

i.e. $$\rho_{\perp c} = \frac{1}{\sigma_{11}}$$

$$\rho_{\parallel c} = \frac{1}{\sigma_{33}}$$

Eq. (3-4) does not have such a simple form of solution if resistivities in any other directions are required.

Because of their highly anisotropic crystal structure, it is to be expected that $\rho_{\parallel c}$ and $\rho_{\perp c}$ will be radically different in the case of the layer structures.

3.2 Experimental

The as-grown crystals were of the order of 0.1mm thick and so it was not possible to use the conventional geometry to measure $\rho_{\parallel c}$. Normal four-probe techniques would have required the longest dimension of the specimen to be parallel to c, clearly impossible in this case. The first attempts to solve this problem are illustrated in figures 3.1 (a) and 3.1 (b). Reproducible results were not obtained with the arrangement of figure 3.1(a) because it was impossible to lay the voltage contact wire exactly in the face of the crystal. The resulting contact resistance often dominated the resistance of the sample, especially at low temperatures.

The ratio of voltage to current was entirely reproducible with the geometry of figure 3.1 (b) but it depended strongly on the distance between the current and voltage contacts on each of the faces of the crystal. Relating the ratio voltage/current to the components of the resistivity tensor is very indirect and is derived from the solution of Maxwell's equations with

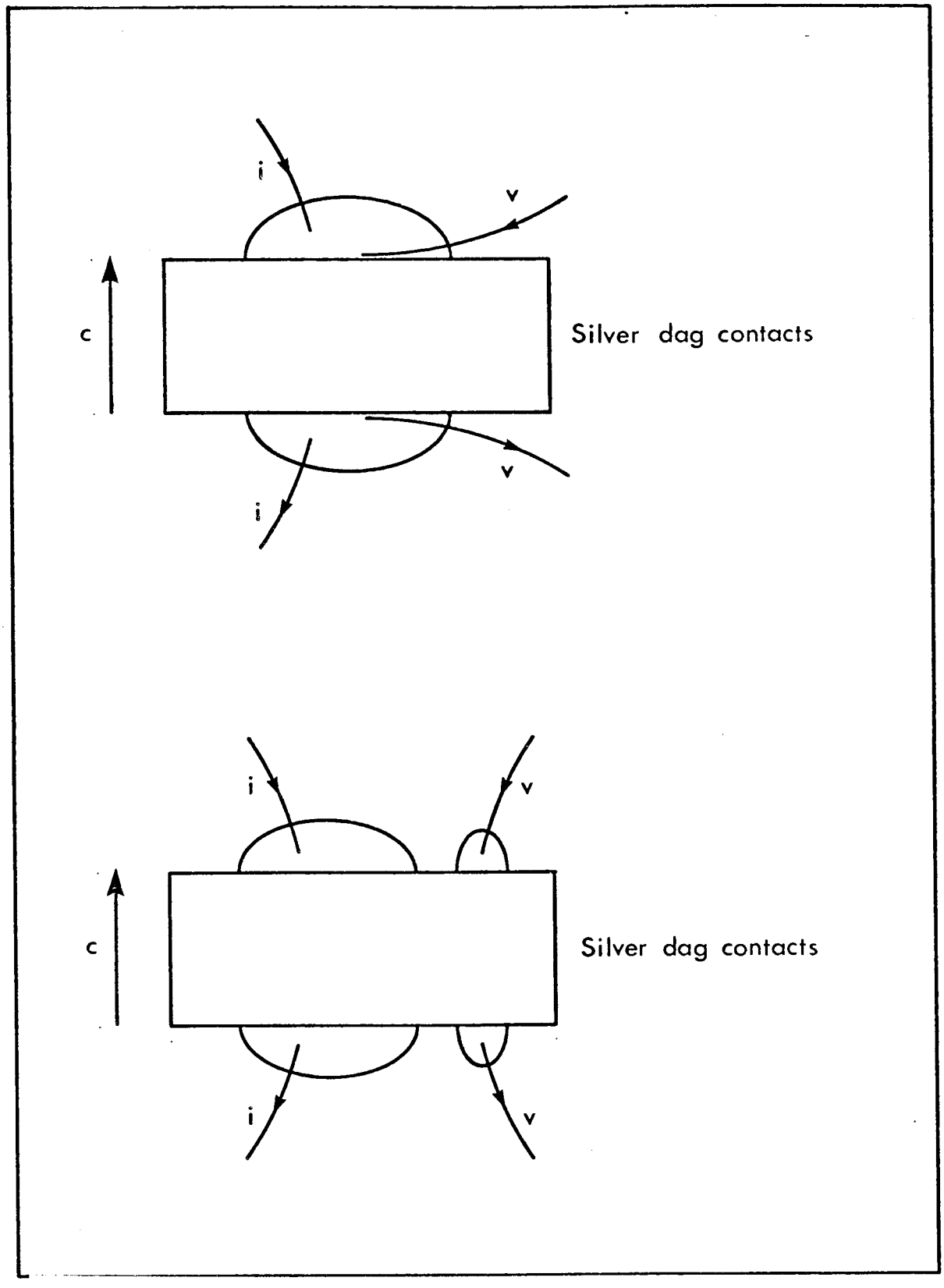

Fig. 3.1 (a) and (b). Two contact geometries that proved unsuccessful for the measurement of the resistivity of $NbSe_2$ perpendicular to the layers.

the appropriate boundary conditions. The calculation has been done for the case of cylindrical symmetry (Primak 1954) and for the case of four point contacts on the top face of a rectangular sample by Soonpaa (1962). The as-grown crystals were not cylindrically symmetric and it was felt that they were too brittle to be lapped into the right shape. There would be too many strains introduced, as well as damage to the crystal edges. A more direct method was therefore used, based on the special properties of the layer structures.

All the layered transition metal dichalcogenides have a definite cleavage plane perpendicular to the c-axis. A scalpel, razor blade, pin or even scotch tape can be used to cleave the crystals. Complete cleaving has been used to prepare crystals of thickness as low as a few unit cell layers (Frindt 1966). A partial cleaving of a thin section of the niobium selenide makes it possible to prepare probes that give a direct measurement of the voltage drop across the crystal. Figure 3.2 shows the arrangement used. The thickness of the voltage probe in relation to the sample thickness is exaggerated for clarity, since in practice the voltage probe is only a few microns thick while the sample is of the order of 0.1mm thick.

A crystal (#1 in figure 3.3) was taken and its resistance measured at room temperature, first with a small contact area, and then with a large contact area. It was found that a consistent value for resistivity followed only if the contact area A,

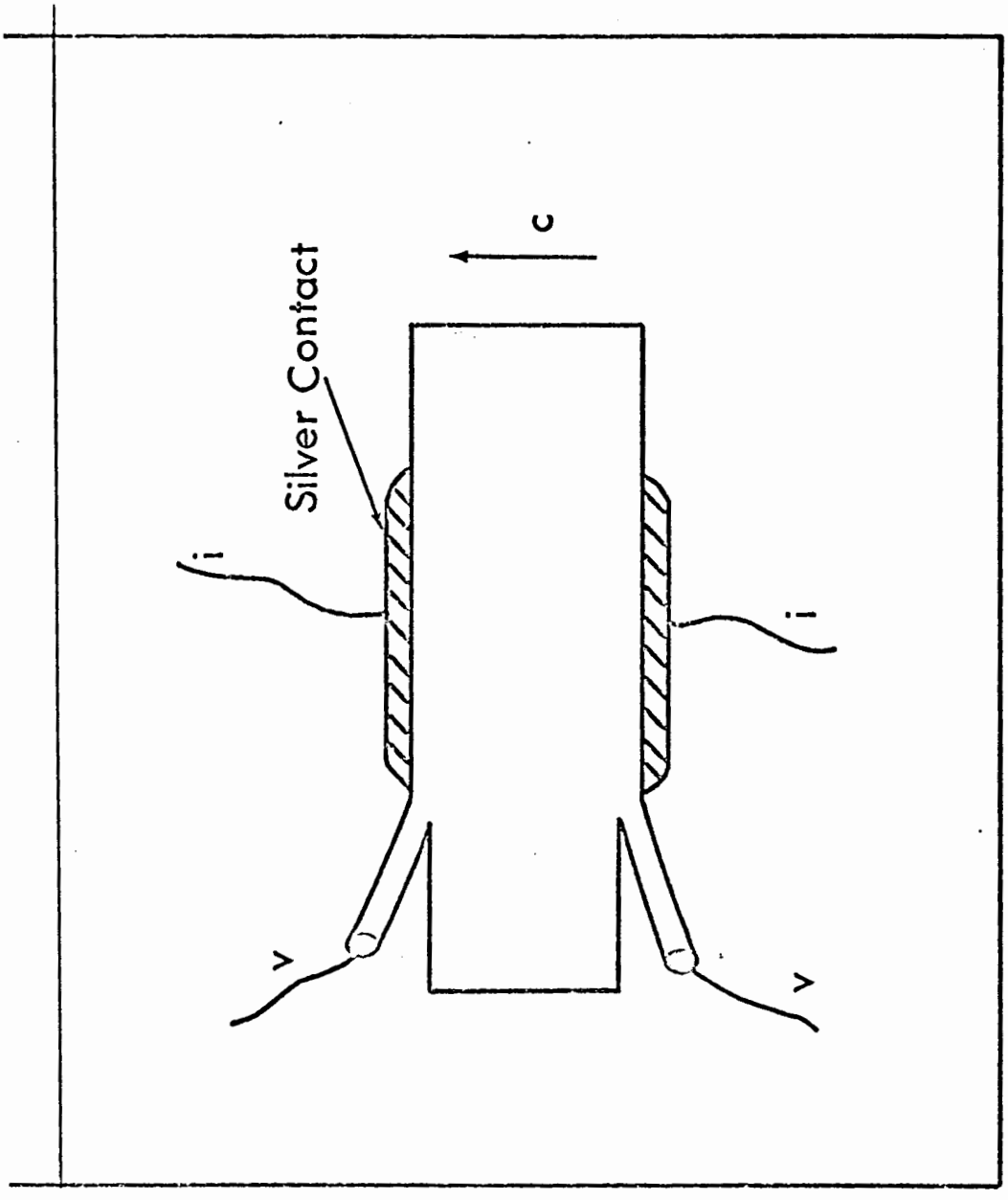

Fig. 3.2 Arrangement of contacts for the measurement of the resistivity of $NbSe_2$ perpendicular to the layers. (Thickness is exaggerated for clarity)

and not the sample area A', was used in the elementary formula $\rho = \frac{RA}{\ell}$. Measurements then followed at room temperature on a series of crystals of varying thickness, including some that were successive cleavings off one thick crystal. Measured resistivity $\frac{RA}{t}$ was plotted against thickness t and is shown in figure 3.3. For the thicker crystals the quantity measured was a combination of $\rho_{\parallel c}$ and $\rho_{\perp c}$ since the current flow is not perfectly parallel to c. Figure 3.4a shows the spreading of the current in this case. For thinner crystals (below about 0.2mm thick) this spreading effect is negligible as can be seen in figure 3.4b. Thus in these cases $\rho_{\parallel c}$ is the quantity being measured.

The resistivity of thin samples (below 0.2mm thick) was measured as a function of temperature from 7°K to 300°K. Temperatures from 77°K to 300°K were obtained by the use of standard organic freezing mixtures*, while below 77°K adequate temperature stability was obtained by putting a dipstick in a helium Dewar. All temperatures were measured with a gold-.03% iron/silver normal thermocouple (Berman 1964). The resistivity measurements are shown in figure 3.5.

---

*The freezing mixtures used were as follows:

Isopentane	112.5°K	Formaldehyde	252.0°K
Ethanol	156.0°K	Propane	229.0°K
Acetone	178.0°K	Ice	273.2°K
Dry ice	195.0°K		

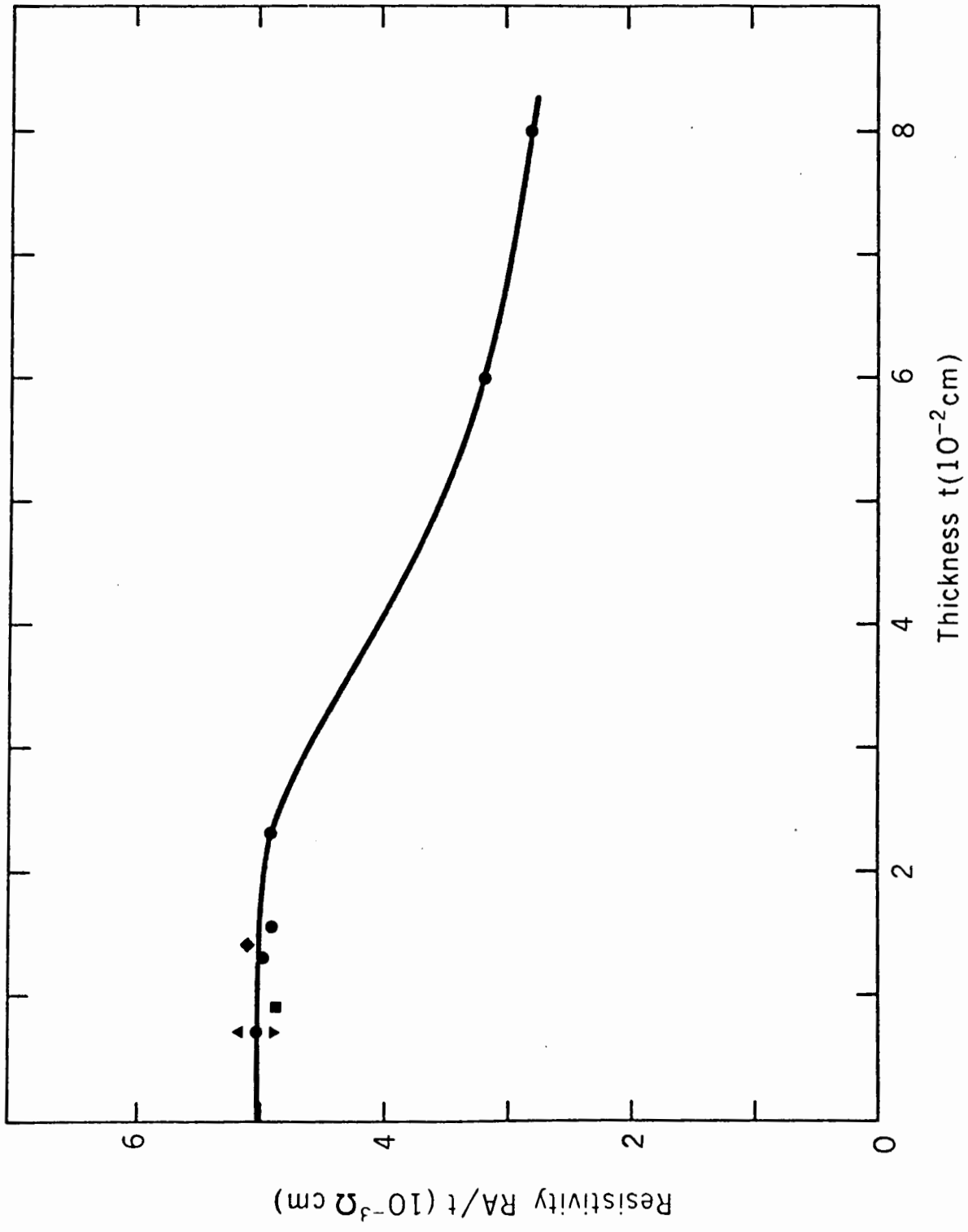

Fig. 3.3 Measured values of the resistivity of $NbSe_2$ for crystals of varying thicknesses. Measurements taken at room temperature.

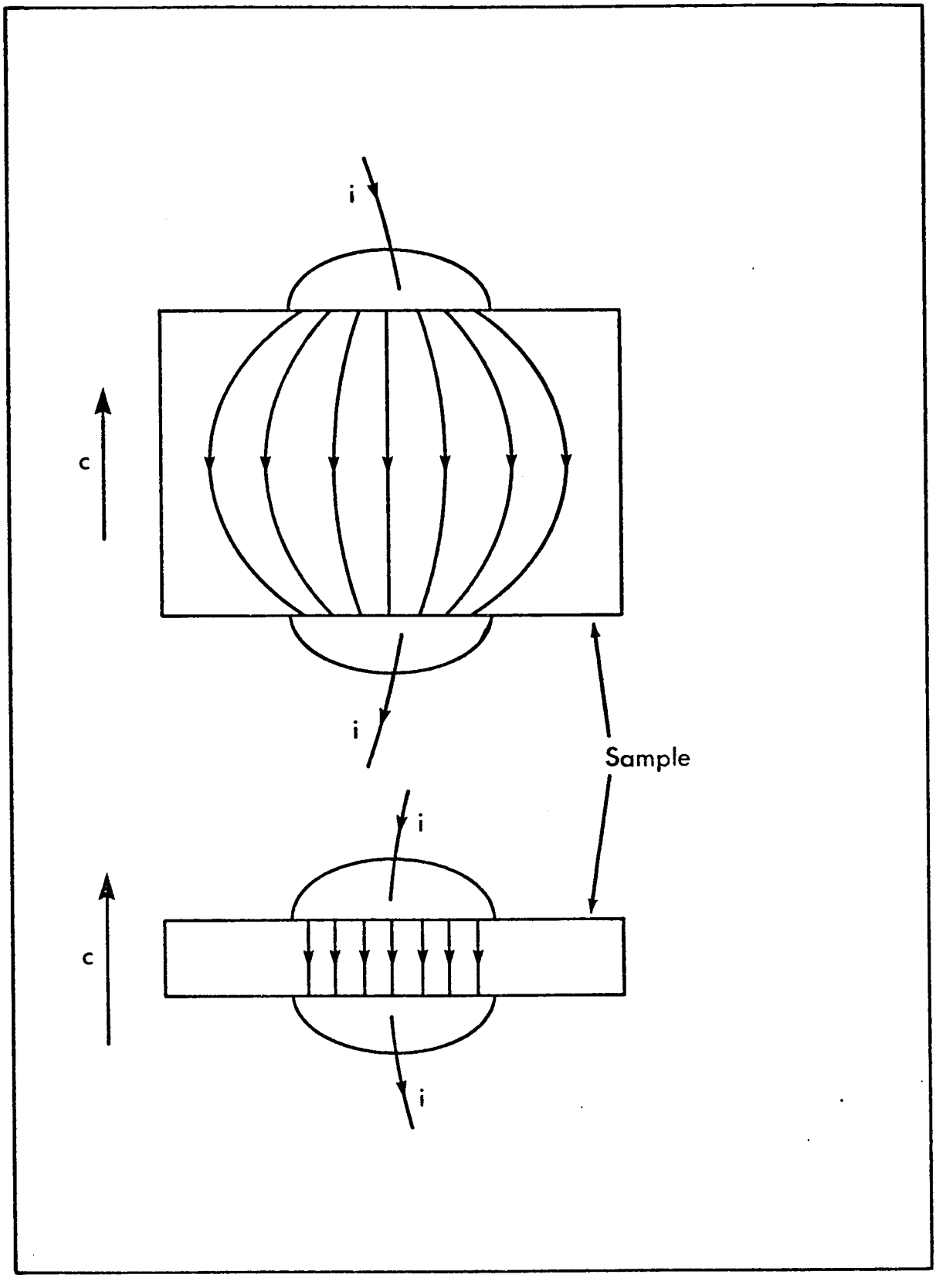

Fig. 3.4 Current streamlines in thin and thick single crystals of $NbSe_2$.

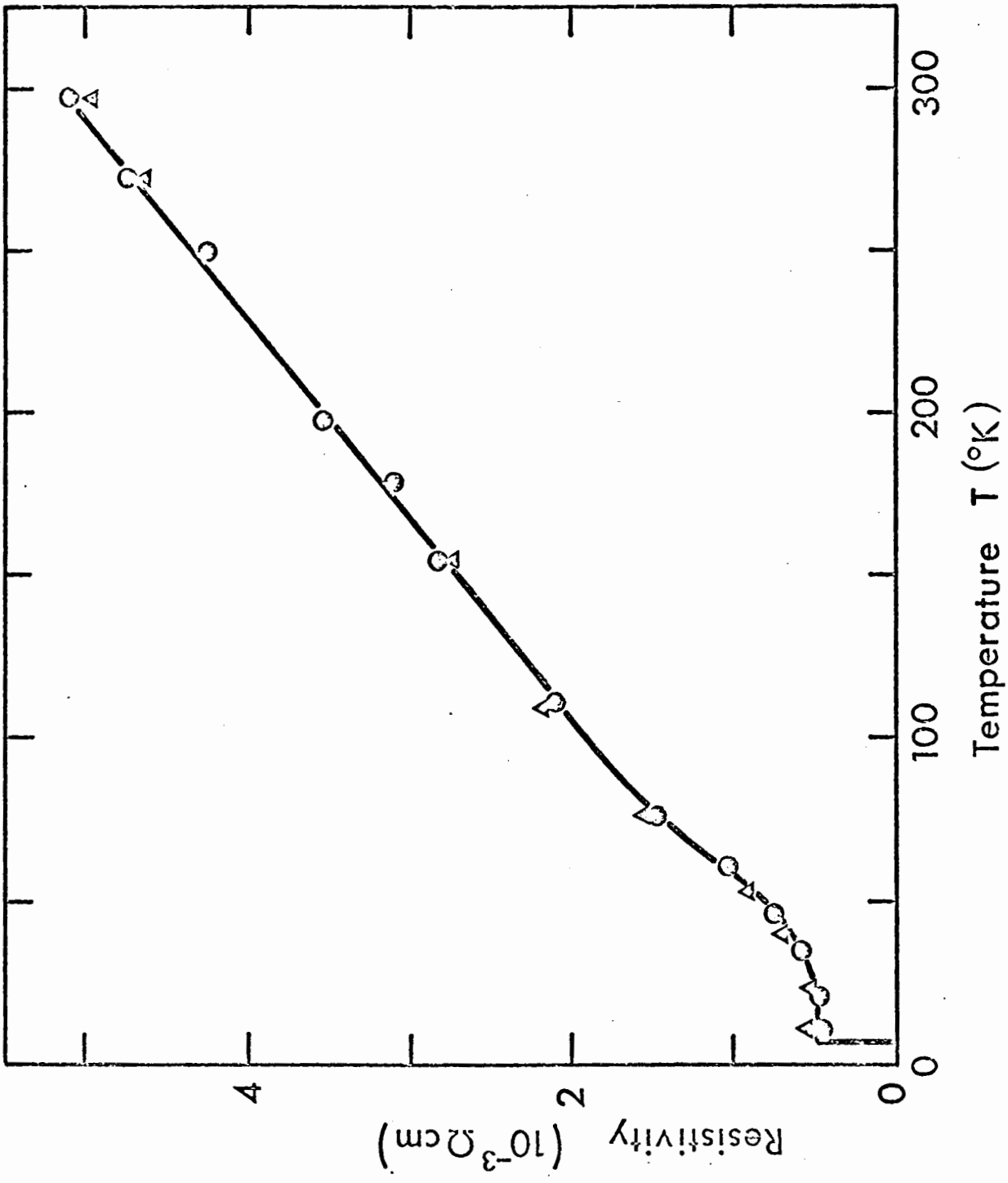

Fig. 3.5 Plot of resistivity parallel to the c-axis of $NbSe_2$ as a function of temperature .

Measurements of $\rho_{\perp c}$ were then taken on the same samples that had been used for the measurements of $\rho_{\parallel c}$. The more regular ones were measured by the conventional four-probe technique, while the irregular ones were measured by the van der Pauw method (van der Pauw 1961). The results for $\rho_{\perp c}$ are in good agreement with those of Lee et al (Lee 1969). Figure 3.6 shows the results of this work and those of Lee et al.

Resistance measurements were made with an Electronics Instruments power supply, giving constant dc currents of 1 ma or less. Voltages and currents were measured with Keithley 150B microvolt-ammeters, except that in later experiments a Tinsley 5590B potentiometer was used for the voltage measurements. Ultimate sensitivity was of the order of 50 nV, being limited by the thermal noise in the silver dag contacts.

3.3 Analysis of results

The high superconducting transition temperature ($7.0^{\circ}K$) makes it very difficult to estimate the residual resistance of the crystal in either direction. As a first approximation the ideal resistivity ρ' was taken to be:

$$\rho'(T) = \rho(T) - \rho(7^{\circ}) \qquad (3\text{-}6)$$

The ideal resistivity given by eq. (3-6) is too low as $\rho(7)$ is clearly an overestimate of the residual resistivity.

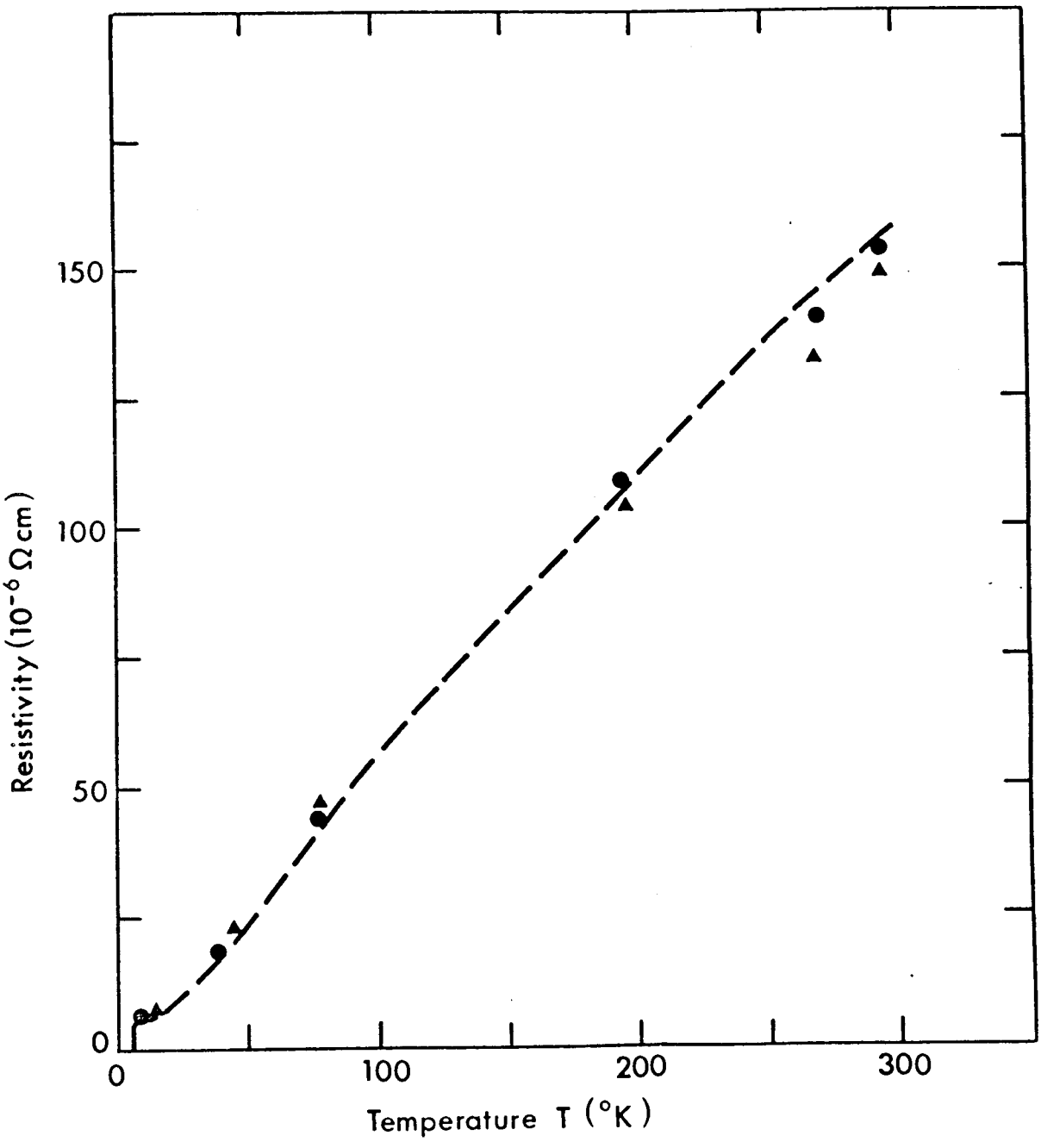

Fig. 3.6 Plot of the resistivity of $NbSe_2$ perpendicular to the c-axis as a function of temperature. The dashed curve shows the results of Lee (1969) .

The systematic error introduced by this approximation must be allowed for in the subsequent discussion.

Figure 3.7 shows the ideal resistivities plotted against temperature. Below 20°K the systematic error introduced by the approximation (3-6) is so large that little reliance can be placed on results in this temperature range. Parallel to c, the ideal resistivity follows a T^3 law in the range 20°K - 60°K and is approximately linear in the range above 100°K. Perpendicular to c the ideal resistivity follows a T^2 law in the range 20°K - 45°K, with an approximately linear dependence above 100°K.

Figure 3.8 shows the ratio of ideal resistivities plotted against temperature. The error bars in figure 3.8 mainly reflect the errors in the estimate of the residual resistivity and in the measurement of the contact area and the crystal thickness. As can be seen from figure 3.8 the ratio of ideal resistivities is constant at 31 : 1 from 300°K to 80°K and then falls linearly with temperature.

At room temperature (295°K) the resistivities are given by:

$$\rho_{\parallel c} = 5.01 \pm 0.20 \times 10^{-3} \text{ ohm cm.}$$

$$\rho_{\perp c} = 1.60 \pm 0.07 \times 10^{-4} \text{ ohm cm.}$$

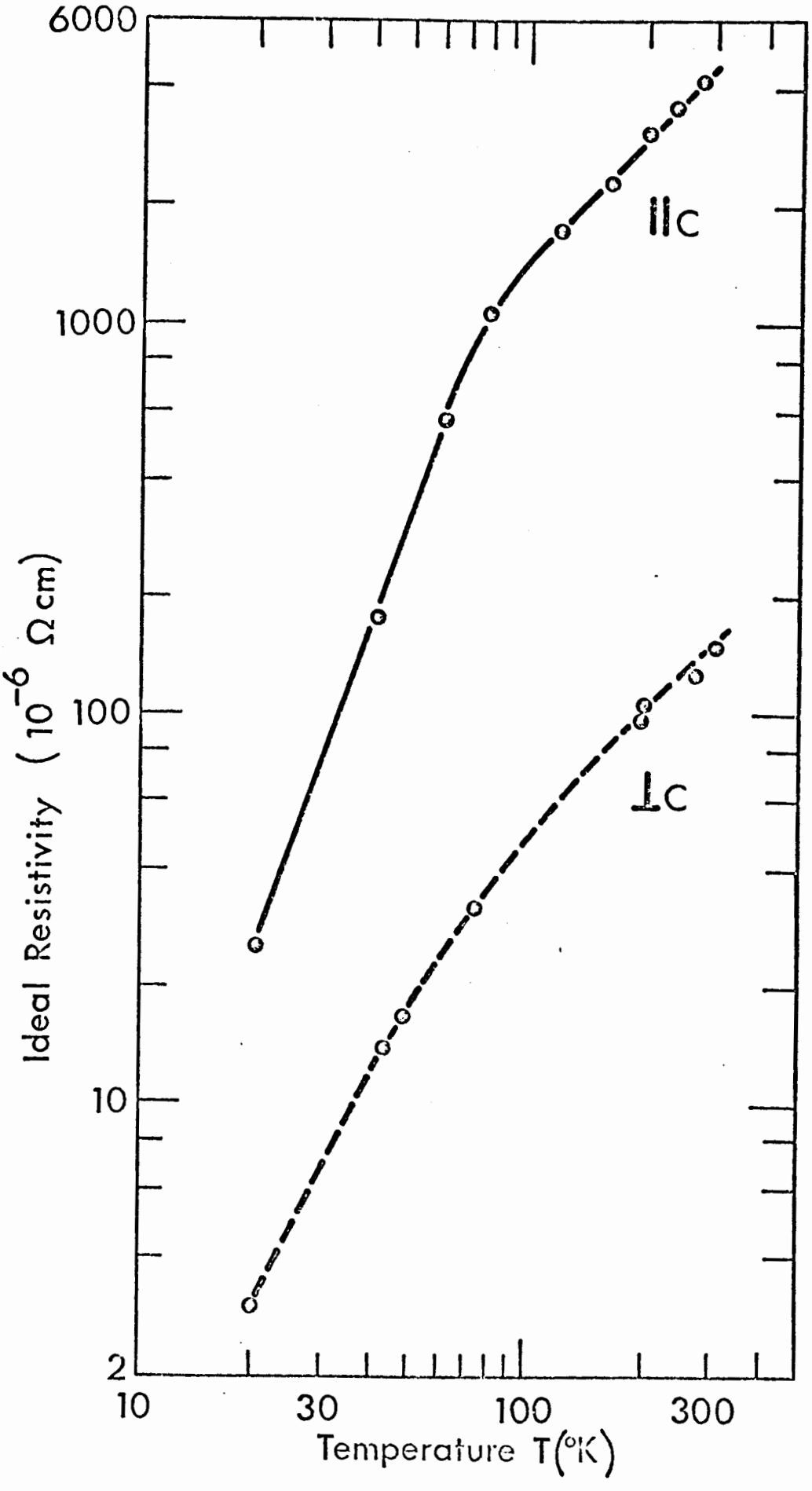

Fig. 3.7 Logarithmic plot of the ideal resistivities of $NbSe_2$

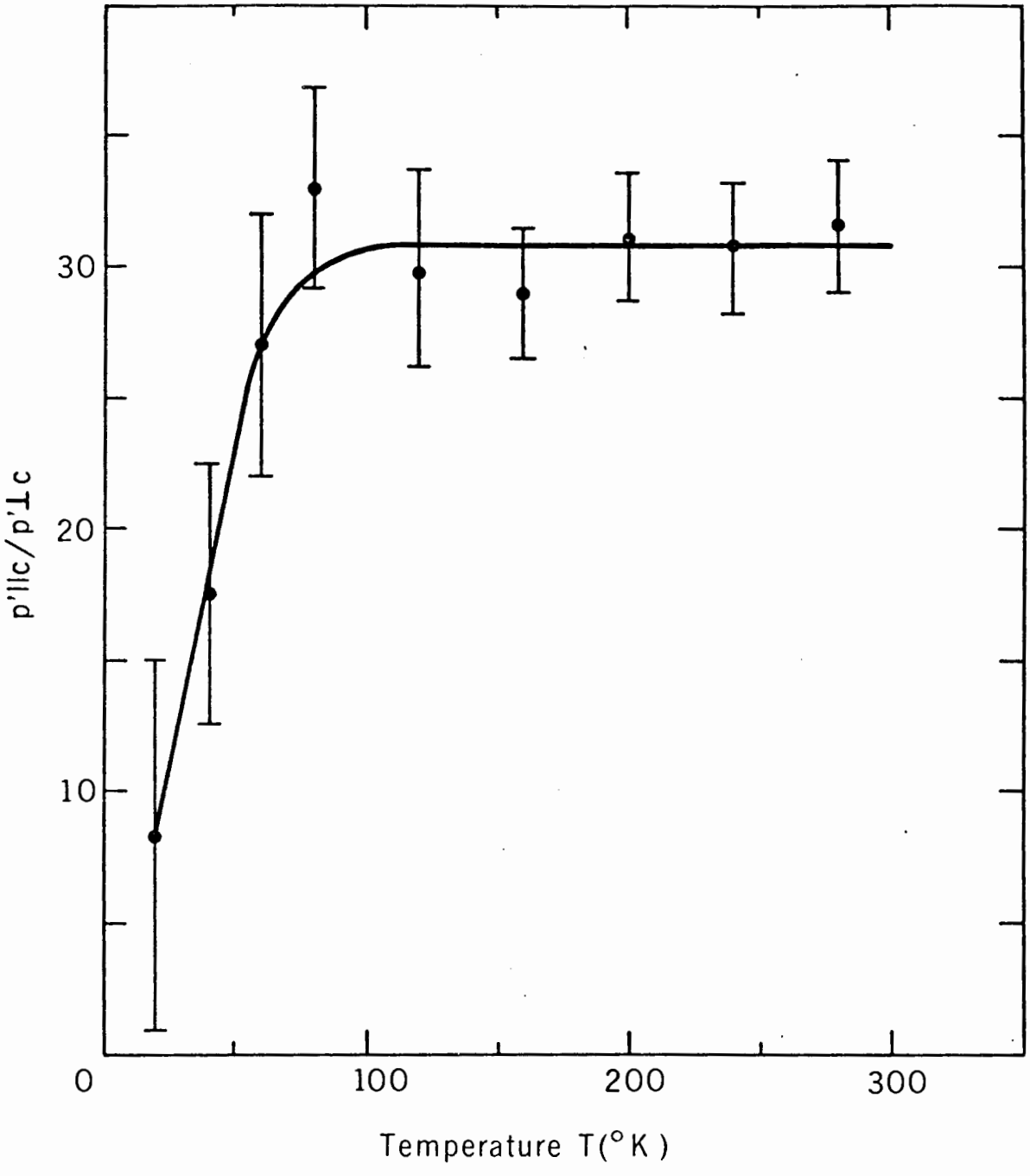

Fig. 3.8 Plot of the ratio of ideal resistivities, $\rho'_{\parallel c}/\rho'_{\perp c}$, as a function of temperature for $NbSe_2$.

Chapter 4 : Single crystal nuclear magnetic resonance measurements on $NbSe_2$

4.1 Motivation

The observed change in the sign of the Hall coefficient in $NbSe_2$ at 26°K (Lee 1969) has led to various explanations being offered. Some of the most likely explanations are summarised below:

a. Cohen et al (1967) proposed a two band model for β-tungsten superconductors that could give p-to-n transitions if there were to be greatly differing densities of states in two bands near the Fermi level. As can be seen from the Goodenough band scheme (1968) shown in figure 4.1, both the bands near E_F are d-bands, and so it is unlikely that the density of states would be radically different in the two bands.

b. Related to this is the possibility that the mobilities of the carriers in the two bands may be very different. Experimentally the direct measurement of band mobilities in metals is very difficult. This model is discussed further in chapter 5 below.

c. Lee (1970) proposed the hypothesis that $NbSe_2$ was antiferromagnetic. The susceptibility measurements needed to test this hypothesis required crystals of a much higher purity than were available, especially with regard to ferromagnetic

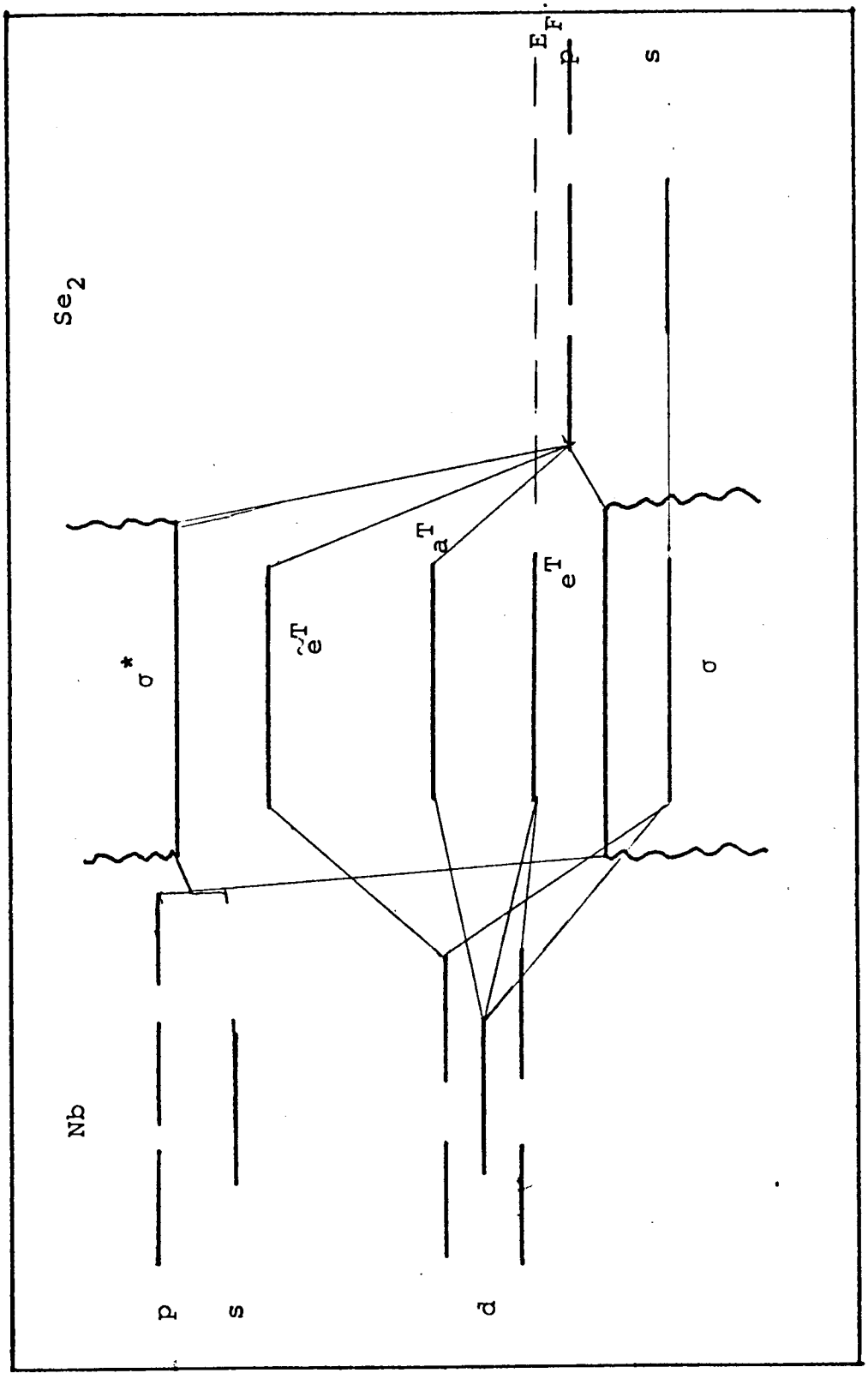

Fig. 4.1 Band structure for $NbSe_2$, after Goodenough (1968) .

impurities.

d. X-ray diffraction studies (Geballe 1971) show a very small change in lattice parameters of the order of 0.3%. This may be indicative of a phase change in $NbSe_2$, and this could be detected in various ways, an obvious possibility being nuclear magnetic resonance.

e. The electronic structure of the niobium atom may change from 77°K to 7°K. This would alter the intensities of the X-ray diffraction pattern (Kittel 1966, pp. 66-68) through the atomic scattering factor, but there was not readily available X-ray diffraction apparatus sufficiently sensitive to resolve minor changes in intensities. However changes in the charge distribution around the niobium nucleus result in changes in the electrostatic field gradient at the Nb^{93} nucleus. Thus the use of nuclear magnetic resonance methods can test for any changes in electronic structure below 77°K.

4.2 Theory of electric quadrupole interactions

The treatment follows closely that of Slichter (1963).

Classically the interaction energy between a charge distribution $\rho(\underline{r})$ and an external potential $V(r)$ is

$$E = \int \rho(r)\, V(r)\, d\tau \qquad (4.1)$$

Expanding $V(\underline{r})$ as a Taylor series about the origin and substituting into equation 4.1 results in

$$E = V(0)\int \rho d\tau + \sum_{i=1}^{i=3} V_i \int X_i \rho d\tau + \frac{1}{2!}\sum_{i,j} V_{ij} \int X_i X_j \rho d\tau + \ldots\ldots \tag{4.2}$$

WHERE $V_i = \left.\frac{\delta V}{\delta X_i}\right|_0$, $V_{ij} = \left.\frac{\delta^2 V}{\delta x_i \delta x_j}\right|_0$

For the case of a nucleus situated at the origin, the first term considers the nucleus as a point charge. The second term is the electric dipole term, and this is zero for a nucleus in equilibrium. The third term is the electric quadrupole term and it may be simplified by referring to the principal axes of the nucleus.

$$V_{ij} = 0 \quad \text{if} \quad i \neq j \tag{4.3}$$

and

$$\sum_i V_{ii} = 0 \tag{4.4}$$

Equation 4.4 holds as V satisfies Laplace's equation in the absence of external charges.

Equations 4.3 and 4.4 reduce the number of independent elements of the quadrupole term from nine to two.

Define the quadrupole tensor Q_{ij}

$$Q_{ij} = \int \left[3X_i X_j - \delta_{ij} r^2 \right] \rho d\tau$$

$$\therefore \int X_i X_j \rho d\tau = \frac{1}{3}\left[Q_{ij} + \int \delta_{ij} r^2 \rho d\tau \right]$$

quadrupole energy E_2

$$= \frac{1}{2} \sum_{i,j} V_{ij} \int X_i X_j \rho d\tau \qquad (4.5)$$

$$= \frac{1}{6} \sum_{i,j} \left(V_{ij} Q_{ij} + V_{ij} \delta_{ij} \int \rho r^2 d\tau \right)$$

By virtue of equation 4.4, the second term vanishes

$$\therefore E_2 = \frac{1}{6} \sum_{i,j} V_{ij} Q_{ij} \qquad (4.6)$$

To get a quantum-mechanical expression for the quadrupole Hamiltonian, ρ and Q_{ij} must be replaced by the corresponding operators.

$$\rho = |e| \sum_{\substack{\text{protons} \\ t}} \delta (\underline{r} - \underline{r}_t) \qquad (4.7)$$

as the charges are located on the protons of the nucleus. Each proton is considered as a point charge at r_t.

$$Q_{ij} = \int \left(3 X_i X_j - \delta_{ij} r^2 \right) \rho d\tau \qquad (4.8)$$

$$= |e| \sum_t \left(3 X_{it} X_{jt} - \delta_{ij} r_t^2 \right)$$

Thus the quadrupole Hamiltonian is

$$H_Q = \frac{1}{6} \sum_{i,j} V_{ij} Q_{ij} \qquad (4.9)$$

with Q_{ij} given by equation 4.8.

The Wigner-Eckart theorem makes it possible to expand any function of operators in terms of a sum of the irreducible representations of the symmetry group of the system under consideration. Thus for a nucleus of total spin I, the quadrupole term in equation 4.8 can be put in terms of the matrix elements of the total spin I^2 and the spin along one of the axes of the nucleus.

It is shown (Slichter 1963, p. 170) that $\langle Im | Q_{ij} | Im' \rangle$, the matrix element linking a state with spin $m\hbar$ along an axis to a state with spin $m'\hbar$ along the same axis is related to the I's by

$$\langle Im | Q_{ij} | Im' \rangle = \langle Im | |e| \sum_t 3X_{it} X_{jt} - \delta_{ij} r_t^2 | Im' \rangle$$

$$= C \langle Im | \tfrac{3}{2}(I_i I_j + I_j I_i) - \delta_{ij} I_i^2 | Im' \rangle \qquad (4.10)$$

The proof of equation 4.10 is omitted as only the result is needed. The constant C can be evaluated by taking the

special case of $i=j=z,\ m=m'=I$. Then defining the quadrupole moment Q of the nucleus by

$$eQ = \langle II | \sum_t 3 Z_t^2 - r_t^2 | II \rangle \tag{4.11}$$

Combination of equations 4.10 and 4.11 for the special case yields

$$\begin{aligned} eQ &= C\langle II | \tfrac{2}{3}[I_z^2 + I_z^2] - I^2 | II \rangle \\ &= C[3I^2 - I(I+1)] \\ \therefore C &= \frac{eQ}{2I(2I-1)} \end{aligned} \tag{4.12}$$

and

$$\langle Im | H_Q | Im' \rangle = \frac{eQ}{6I(2I-1)} \langle Im \sum_{i,j} V_{ij} (\tfrac{3}{2}(I_i I_j + I_j I_i) - \delta_{ij} I^2 | Im' \rangle \tag{4.13}$$

Equation 4.13 results from the combination of equations (4.6), (4.8), (4.10) and (4.12).

$$H_Q = \frac{eQ}{6I(2I-1)} \sum_{i,j} V_{ij} (\tfrac{3}{2}[I_i I_j + I_j I_i] - \delta_{ij} I^2) \tag{4.14}$$

Referred to the principal axes of the nucleus (4.14) simplifies further to (using Laplace's equation $\Sigma_{ii} V_{ii} = 0$)

$$H = \frac{eQ}{4I(2I-1)} \left[V_{zz}(3I_z^2 - I^2) + (V_{xx} - V_{yy})(I_x^2 - I_y^2) \right] \tag{4.15}$$

Define the field gradient $eq = V_{zz}$ (4.16)

the asymmetry parameter $\eta = \frac{V_{xx}-V_{yy}}{V_{zz}}$ (4.17)

In terms of eq and η , equation 4.15 becomes

$$H_Q = \frac{e^2qQ}{4I(2I-1)}\left[(3I_z^2-I^2)+\tfrac{1}{2}\eta\left[I_+^2-I_-^2\right]\right] \tag{4.18}$$

$NbSe_2$ has a symmetry axis along the z-axis and so the case of $\eta = 0$ applies here

$$H_Q = \frac{e^2qQ}{4I(2I-1)}\left[3I_z^2-I^2\right] \tag{4.19}$$

Consider a magnetic field H_o applied to a nucleus of spin I. The field is along the direction of the symmetry axis of the nucleus. (The case of the magnetic field and the nuclear symmetry axis in different directions is treated in appendix A). Then the Zeeman part of the total Hamiltonian $\mathcal{H}$ commutes with the quadrupolar part and an exact solution of the Schrodinger equation is possible.

$$\mathcal{H} = -\gamma_n \hbar H_0 I_z + \frac{e^2qQ}{4I(2I-1)}(3I_z^2 - I^2) \tag{4.20}$$

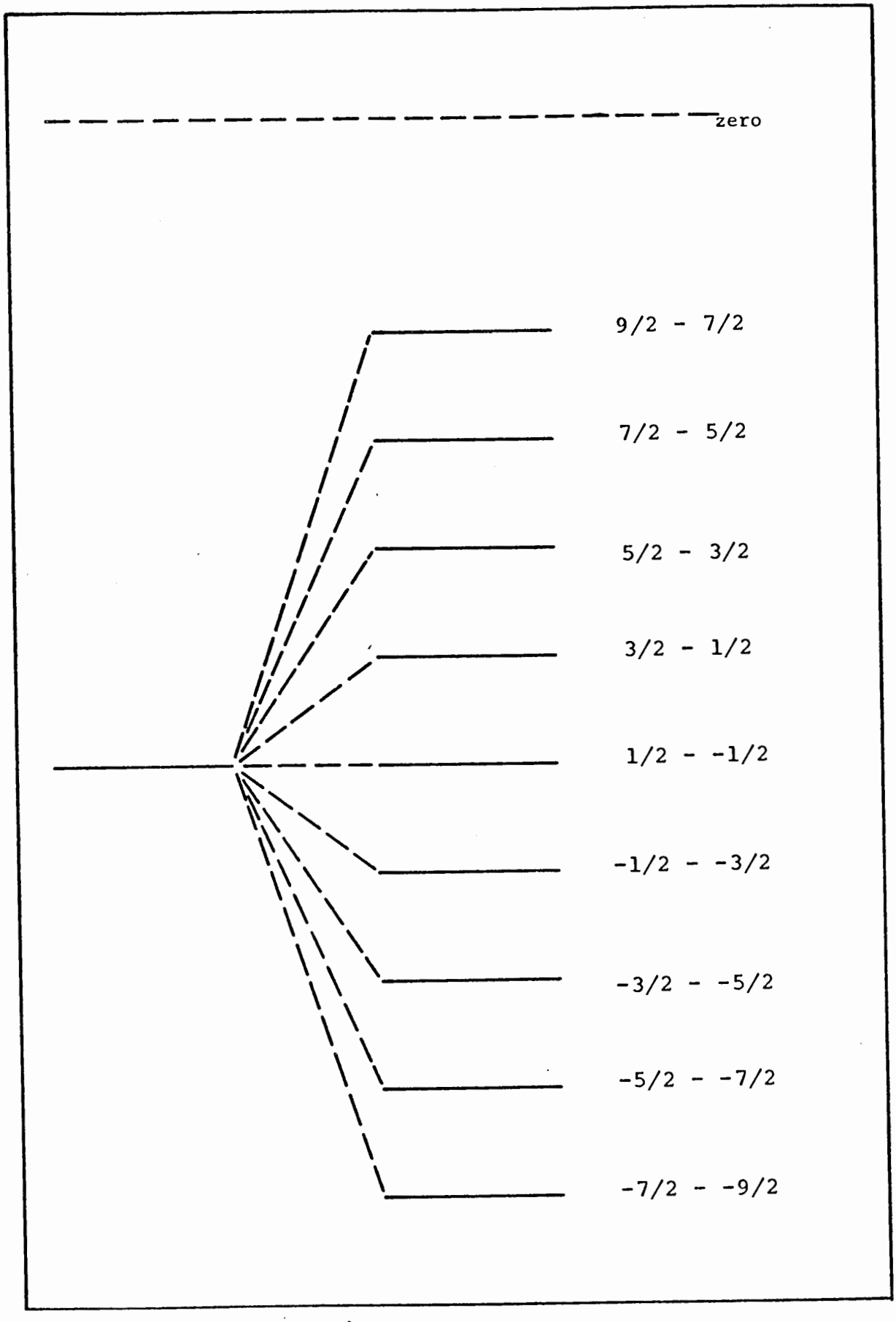

Fig. 4.2 Frequencies of the allowed transitions of a nucleus of spin 9/2 and quadrupole moment Q in a magnetic field. The separation of each pair of lines is $e^2qQ/24$.

where γ_n is the gyromagnetic ratio of the nucleus.

$$\therefore E_m = \langle m | \mathcal{H} | m \rangle$$

$$= \langle m | -\gamma_n \hbar H_0 I_z + \frac{e^2qQ}{4I(2I-1)}(3I_z^2 - I^2) | m \rangle \qquad (4.21)$$

$$= -\gamma_n \hbar H_0 m + \frac{e^2qQ}{4I(2I-1)}\left[3m^2 - I(I+1)\right]$$

For a nucleus such as Nb^{93}, with a spin of $\frac{9}{2}$ the energy level scheme is as shown in figure 4.2. The separation of the $\frac{3}{2} - \frac{1}{2}$ and $\frac{1}{2} - -\frac{1}{2}$ lines gives a direct measurement of the quadrupole coupling constant e^2qQ.

4.3 Experimental*

The block diagram of the spectrometer used is shown in figure 4.3. The sample was placed in a coil, and the coil linked to the marginal oscillator by a 3/8" stainless steel coaxial cable. The marginal oscillator was a modified Pound-Knight box (Pound 1950, Sharma 1967) and the resonance was

---

* This work was carried out in the Department of Physics, University of British Columbia, using the facilities of Dr. D. Williams and the assistance of Dr. J. Trodahl and Mr. J. Schratter.

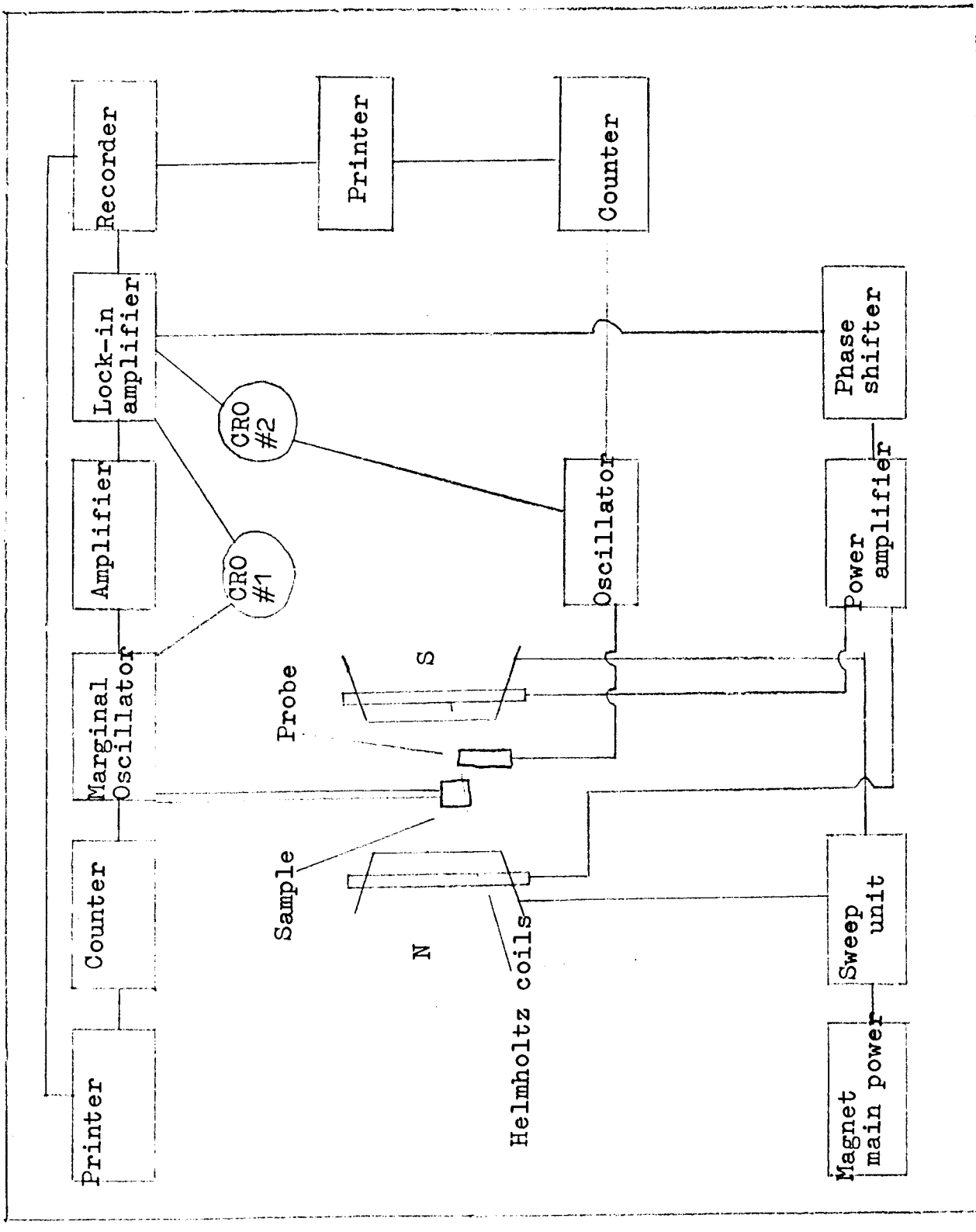

Figure 4.3 Block diagram of N.M.R. spectrometer

observed by monitoring the changes in output level of the oscillator as the magnetic field was swept. The output from the oscillator was fed into a narrow band amplifier and then a phase-sensitive detector (P.A.R. type HR-8) tuned at 38 Hz. The output of the phase sensitive detector was fed into a recorder (Hewlett Packard model 7101A). The 12" Varian magnet provided a static magnetic field of between 5 and 11 kilogauss, with field stability of 1 part in 10^4 over a period of 1 hour and a field homogeneity of better than 0.1 gauss/cm near the centre of the pole faces. The magnetic field was modulated at 38 Hz by putting the amplified reference signal of the lock-in amplifier on to two Helmholtz coils attached to the pole faces of the magnet. The amplitude of the modulation was 8 gauss peak-to-peak. The sweep of the field was obtained by using a motor-driven helipot between the main magnet power supply and the main magnet coils.

The frequency of the marginal oscillator was monitored continually and the output of the frequency counter was recorded on the printer. The oscillator frequency was constant to 1 part in 10^4 at constant temperature, but was very sensitive to temperature drift. The static magnetic field was measured by using a glycerol probe. A glass tube was filled with glycerol and then sealed. A few turns of copper wire were wound round it and the coil connected to an oscillator by means of a coaxial cable. The oscillator could be tuned to a range of frequencies

and the fine tuning control gave a sensitivity of 1 part in 10^5 or thereabouts. The proton resonance of the glycerol was observed and the frequency measured on a counter. The counter output was then printed out and recorded by actuating an event marker on the recorder*. As the gyromagnetic ratio of the proton is known to a high degree of accuracy, a measurement of the proton resonance frequency served as an accurate determination of the static magnetic field. As a precaution the glycerol probe was put in the same position in the field for all experiments so that the error due to field inhomogeneities was constant from run to run.

In this way the Nb^{93} frequency and static magnetic field at resonance could be measured. This gave the gyromagnetic ratio for the Nb^{93} nucleus in $NbSe_2$. This was done for the Nb^{93} $\frac{1}{2} - -\frac{1}{2}$ and the Nb^{93} $\frac{3}{2} - \frac{1}{2}$ lines.

The experiments were carried out with the magnetic field parallel to the c-axis of the $NbSe_2$ single crystal. Initial orientation was done optically, using reflection from the mirror faces perpendicular to the c-axis. The sample was then enclosed in a sealed outer shield and the angle of the magnet adjusted until the frequency of the Nb^{93} resonance $\frac{3}{2} - \frac{1}{2}$

---

* An alternative to the recorder is to use an X-Y recorder, with the proton frequency on the X-axis and the marginal oscillator output on the Y-axis. In this way interpolation between event marker signals is avoided.

was a minimum. This ensured that the magnetic field was aligned parallel to the c-axis of the sample. (See appendix A for a proof of this).

The temperature control for the experiments was as in figure 4.4. The carbon resistor acted as a sensor and the error signal from an Oxford Instruments resistance bridge fed current to the heater. Thus the heater served to keep the carbon resistor at a constant resistance, and so kept the temperature constant. With this system the temperature control was better at lower temperatures as the resistance of the carbon resistor used changed more rapidly at low temperature than at high temperature. In all cases the temperature was held constant to within 0.5°K over the one hour period needed to sweep through the resonance. Exchange gas was used to obtain temperatures in the range from 7°K to 18°K. Above 18°K the sample was in vacuum, so that the heater currents needed to maintain relatively high temperatures were reduced, with consequently smaller helium boil off. Temperatures were measured using a gold-iron/silver normal thermocouple (Berman 1964) with the reference at liquid helium temperature (4.2°K). The thermocouple voltage was measured directly with a Keithley model 148 nanovoltmeter.

4.4 Data treatment and results

The radio frequency magnetic field from the marginal

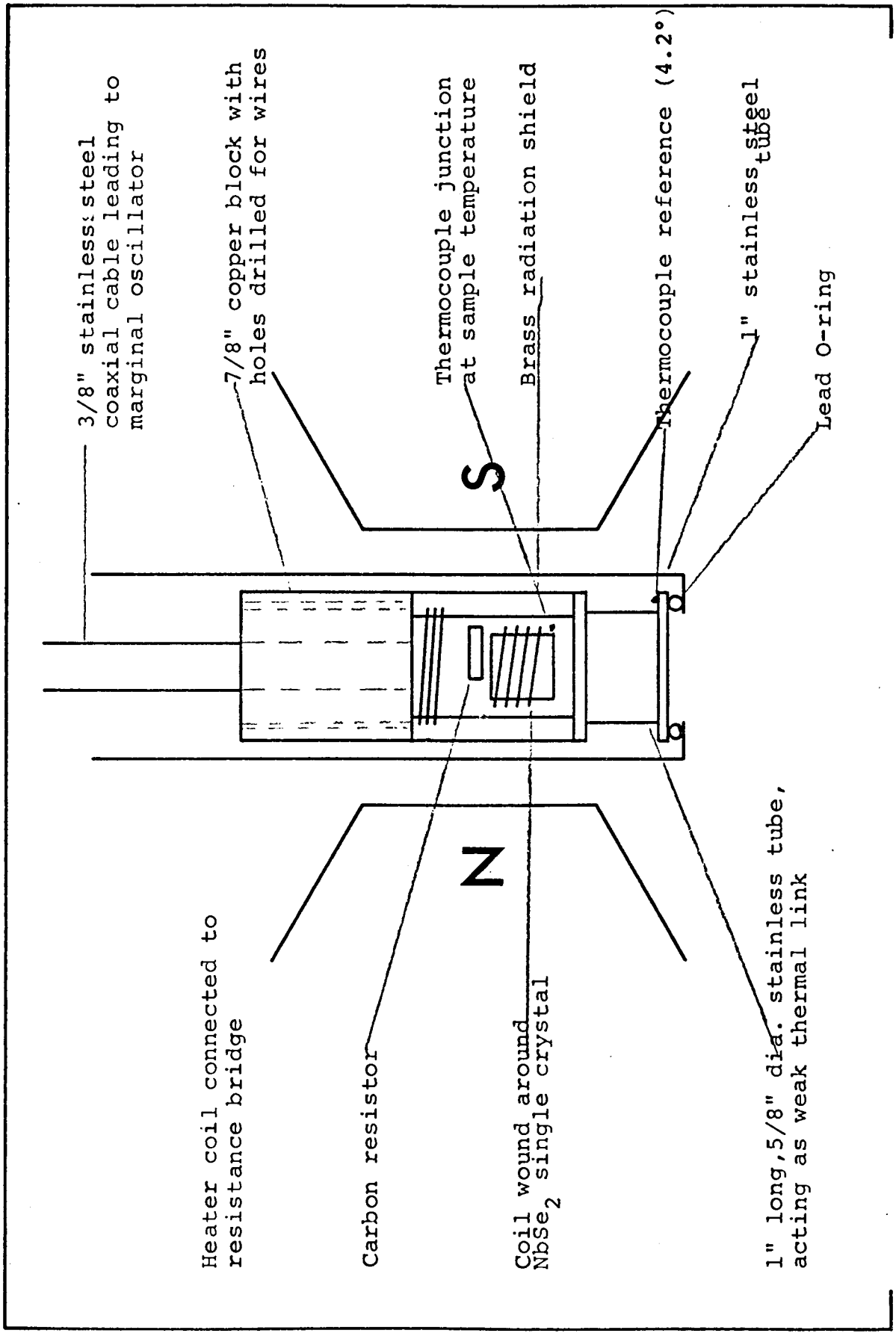

Fig. 4.4 Temperature control system for NMR measurements on $NbSe_2$ single crystals at temperatures between 7°K and 77°K

oscillator excites the resonance, but it also sets up eddy currents in the metallic $NbSe_2$. The lock-in amplifier output records the first derivative of the power absorbed by the sample. The power absorbed has been calculated (Chapman 1957) in closed form for a flat plate of thickness 2t and skin depth δ. For $2t \gg \delta$ the output of the lock-in is given by

$$p = \frac{d}{dn}\left[\frac{X' + X''}{D}\right] \qquad (4.22)$$

where X', X'' are the real and imaginary parts of the susceptibility, n is the displacement from centre of the Gaussian line of unit linewidth $y = \exp\left[\frac{1}{2}n^2\right]$, and D is a normalising factor.

For a sample thick compared to the skin depth, and whose resonance has a Gaussian line shape the lock-in output is as shown in figure 4.5. The resonance field H_R and the linewidth ΔH_L are given by

$$H_R = H_{MAX} + 0.79\ [\ H_{MAX} - H_{MIN}\ ] \qquad (4.23)$$

$$\Delta H_L = 0.68\ (H_{MAX} - H_{MIN}) \qquad (4.24)$$

For a metal the skin depth is given by

$$\delta = \frac{C}{(2\pi\omega\sigma)^{\frac{1}{2}}} \qquad (4.25)$$

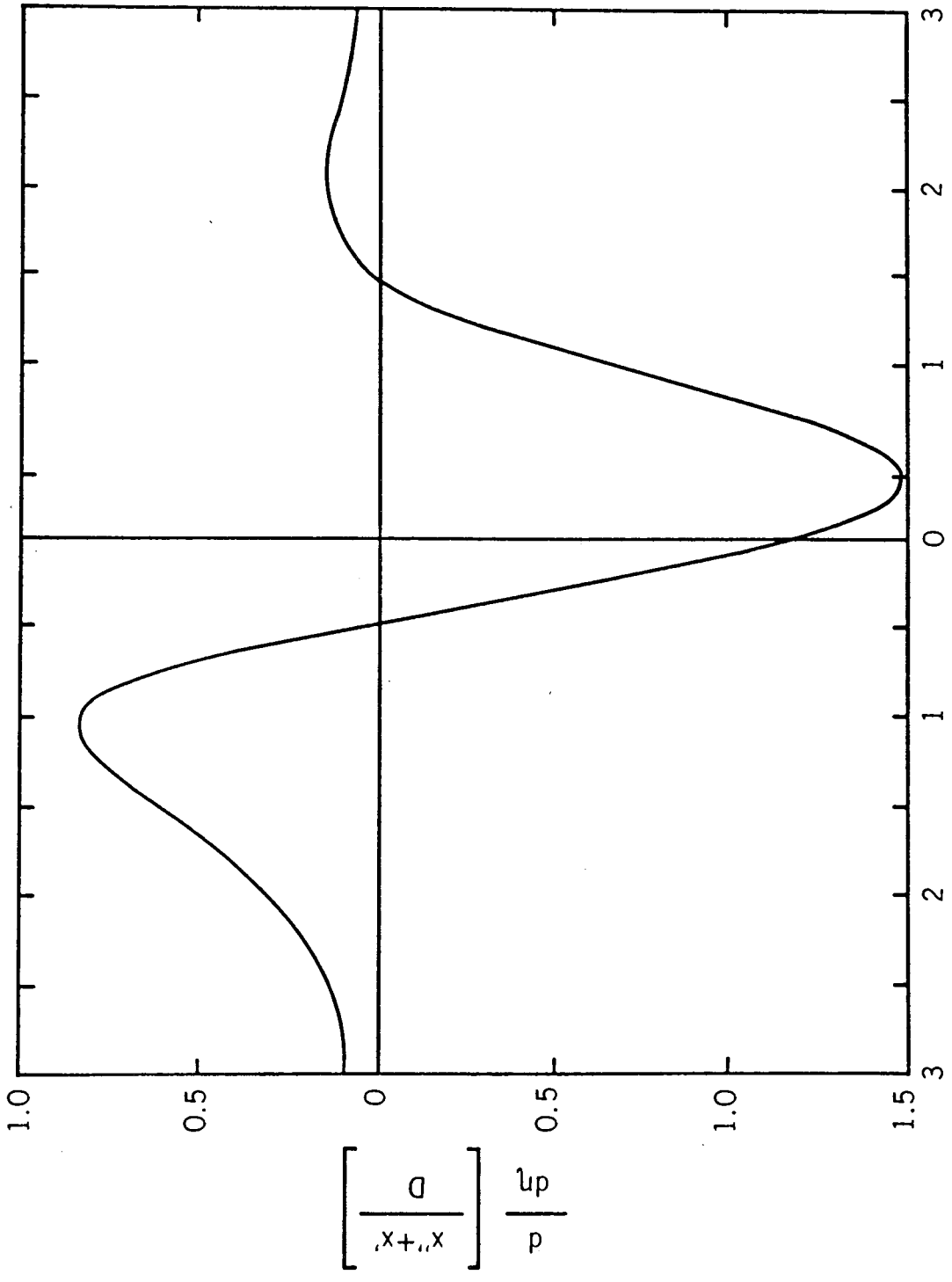

Fig. 4.5 Shape of the absorption line for the Nb^{93} resonance in $NbSe_2$ (after Chapman (1957)) .

where ω = angular frequency and σ = conductivity.

Rewritten in more practical units (Chapman 1957)

$$\delta = 5.03 \times 10^{-3}\left(\frac{\rho'}{\nu'}\right)^{\frac{1}{2}} \qquad (4.26)$$

Now for $NbSe_2$ at 77°K ρ' = 50 microhm.cm and ν' = 8 MHz, giving δ = 0.12 mm. For the crystal used t = 0.4 mm, so

$$2t/\delta = \frac{0.8}{0.12} \sim 6.5 \qquad (4.27)$$

Equation (4.27) shows that the use of figure 4.5 to locate the exact centres of resonance lines for $NbSe_2$ is justifiable.

The results obtained at 77°K and a field of 8.294 KG parallel to the c-axis of $NbSe_2$ are shown in Table 4.I. Similar results were obtained at 20.6 KG.

Table 4.I

Nb^{93} resonance 1/2 - -1/2	8.670 MHz
Gyromagnetic ratio for Nb^{93} in $NbSe_2$	10.453 MHz/10KG
Gyromagnetic ratio for Nb^{93} in Nb_2O_5	10.407 MHz/10KG (Sherriff 1951)
Knight shift	0.44 %
Linewidth	8 gauss
Signal-to-noise ratio	8 : 1
Nb^{93} resonance 3/2 - 1/2	6.100 MHz
Quadrupole coupling constant	61.68 MHz
Linewidth	26 gauss
Signal-to noise ratio	2 : 1

Measurements made at 17.7°K gave the following results:

(i) The main line (Nb^{93} 1/2 - -1/2) was broadened to a linewidth of the order of 20 gauss.

(ii) It was not possible to see any satellite lines because of the broadening of all lines at the lower temperature.

Chapter 5 : Discussion

The resistivity measurements described in chapter 3 and the measurement of the Hall effect (Lee 1969, Huntley 1971) provide the basis for a calculation of band mobilities using the model of two conduction bands, one consisting of electrons and one of holes. The nuclear magnetic resonance experiments showed the existence of changes in the conduction band electrons as the temperature was lowered.

5.1 Resistivity of $NbSe_2$

The anisotropic nature of $NbSe_2$ shows itself in the ratio $\rho_{\parallel c}/\rho_{\perp c}$ being considerably greater than one, and also in the ratio being a function of temperature. Above $100^{\circ}K$ (Fig. 3.7) both $\rho'_{\parallel c}$ and $\rho'_{\perp c}$ are linear in T. This behaviour is typical of most metals at high temperatures (Meaden 1965). For $NbSe_2$ the Debye temperature is $210^{\circ}K$ (van Maaren 1969). The low temperature results are reminiscent of those obtained for transition metals, as the strongest temperature variation observed is only $\rho_{\parallel c} \sim T^3$, unlike the T^5 observed in the alkali metals (Wilson 1953, p 279). A full explanation of the low temperature results requires a knowledge of both the Fermi surface and the phonon spectrum of $NbSe_2$.

Some conjectures about the Fermi surface have been made (Wilson and Yoffe 1969) but as yet no experimental

determinations have been carried out. With regard to the phonon spectrum, it has been suggested by Krumhansl and Brooks (1953) for graphite, and for layer structures in general by Newell (1955) that at the lowest temperatures the phonon spectrum resembles that of an anisotropic three dimensional Debye solid, while at higher temperatures the spectrum will, to a good approximation, resemble that of a two-dimensional Debye solid. Experimental confirmations of the Newell theory have been provided by the low temperature specific heat of graphite (De Sorbo 1953, 1958). In the case of graphite, three dimensional character is only observed below 1.5°K. A T^3 dependence has been observed for the lattice specific heat of $NbSe_2$ and other related layer structures below 10°K (van Maaren 1969) so that $NbSe_2$ may resemble a three-dimensional Debye solid below 10°K and a two-dimensional Debye solid in some temperature range above 10°K. At 20°K the resistivities $\parallel c$ and $\perp c$ have different temperature dependences, so that the changeover temperature may be between 10°K and 20°K.

5.2 Conductivity and Hall coefficient using a two band model

A p-to-n transition can occur if the carriers in the two bands near the Fermi level have widely different temperature dependences for their mobilities. Given the Hall coefficient and the conductivity, it is possible, with some simplifying

assumptions, to calculate the mobility of the carriers in each of the two bands. In what follows it is assumed:

(i) that the numbers of carriers per unit volume in each band are equal.

(ii) that the current is carried entirely by holes at some high temperature T_o.

(iii) that the number of carriers in each band does not vary with temperature.

Following the method of Wilson (1953, p. 213):

$$\sigma = |e|[n_h\mu_h + n_e\mu_e]$$
$$R = \frac{|e|[n_h\mu_h^2 - n_e\mu_e^2]}{\sigma^2} \qquad (5.1)$$

AS $n_h = n_e = n$

$$\sigma = n|e|[\mu_h + \mu_e]$$
$$R = \frac{n|e|[\mu_h^2 - \mu_e^2]}{\sigma^2} \qquad (5.2)$$

Solving for μ_h, μ_e in terms of the other variables

$$\mu_h = \tfrac{1}{2}\sigma\left[R + \frac{1}{n|e|}\right] \qquad (5.3)$$

$$\mu_e = \tfrac{1}{2}\sigma\left[\frac{1}{n|e|} - R\right] \qquad (5.4)$$

Now n can be found by using the result of a Hall coefficient determination at the high temperature T_o.

$$R(T_o) = \frac{1}{n|e|} \qquad (5.5)$$

therefore

$$\therefore \mu_h(T) = \tfrac{1}{2}\,\sigma(T)\left[R(T_o)+R(T)\right] \qquad (5.6)$$

$$\mu_e(T) = \tfrac{1}{2}\,\sigma(T)\left[R(T_o)-R(T)\right] \qquad (5.7)$$

Putting σ (T) from this work and R(T) from an unpublished determination by Huntley (1971) on crystals from the same batch, the mobilities of the electron and hole bands are shown in figure 5.1. The results of Lee were not used for R(T) as it was felt that the low-temperature values of σ , R were affected by the precise level of impurity in the sample used.

These results, characterised by the drop in mobility of the holes as the temperature falls below 30^{o}K show that there are errors introduced in making the assumptions. At low temperatures the mobility should be constant as the residual conductivity of a material is temperature independent. For a second approximation it is assumed:

(i) that the number of electrons per unit volume n_e is constant at all temperatures.

(ii) that the number of holes is pn_e, where p is a constant.

Then equations (5.1) and (5.2) become:

$$\sigma = n_e |e| \left[p\mu_h + \mu_e\right] \qquad (5.8)$$

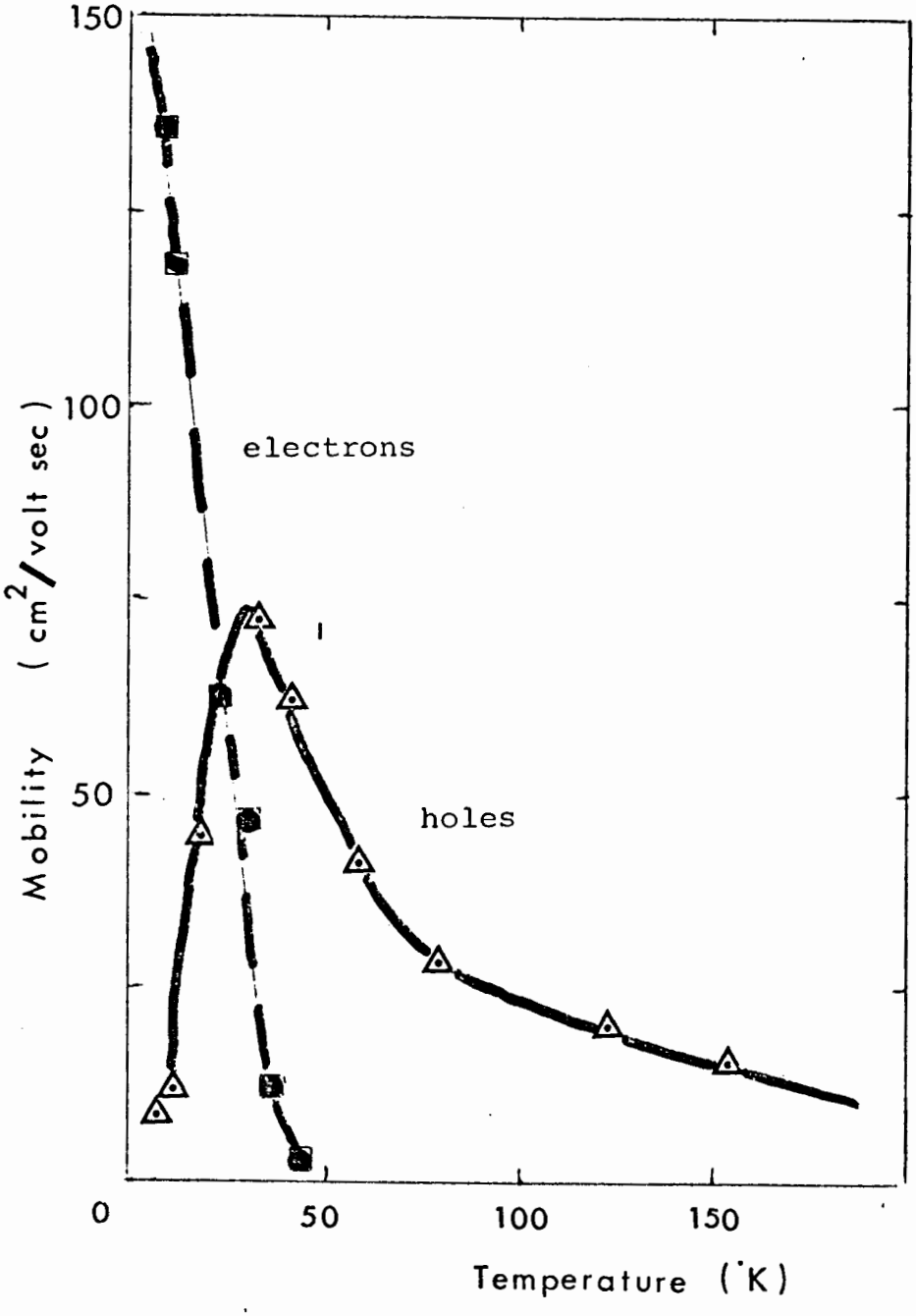

Fig. 5.1 Mobility-temperature curve for $NbSe_2$, calculated on the basis of equal numbers of electrons and holes.

$$R = n_e |e| [\rho\mu_h^2 - \mu_e^2] \qquad (5.9)$$

Equations (5.8) and (5.9) may be combined to give

$$(\rho - \rho^2) \frac{n_e |e|}{\sigma^2} \mu_h^2 + \frac{2\rho}{\sigma} \mu_h - \frac{1}{n_e |e|} - R = 0 \qquad (5.10)$$

$$\mu_e = \frac{\sigma}{n_e |e|} - \rho\mu_h \qquad (5.11)$$

Working in reduced units, $\sigma = \frac{\sigma(T)}{\sigma(280°)}$, $R = \frac{R(T)}{R(280°)}$ the values p = 0.1, $n_e |e| = 0.4$ gave the decreasing functions shown in figure 5.2 for μ_h and μ_e. Other values of p in the range $0.05 \leq p \leq 1$ and $n_e |e|$ in the range $0.2 \leq n_e |e| \leq 2$ gave inadmissible results as μ_h and μ_e were not both positive, strictly decreasing functions of temperature. The reduced units are converted to more practical units by normalising to $\sigma(280°) = 6.6 \times 10^3$ mho.cm^{-1} and $R(280°) = 4.7 \times 10^{-4}$ coul.cm^{-3} (Lee 1969). It will be seen that both μ_h and μ_e are approximately proportional to 1/T, characteristic of metallic mobilities. With this model $n_e = 5.3 \times 10^{21}/cm^3$ * and

---

* With this model n_e is a little high, but these values of p and n_e e do give decreasing mobilities with rising temperature for both bands, and also predicts a very low (about 0.5%) magnetoresistance at 7°K. This is in good agreement with experiment.

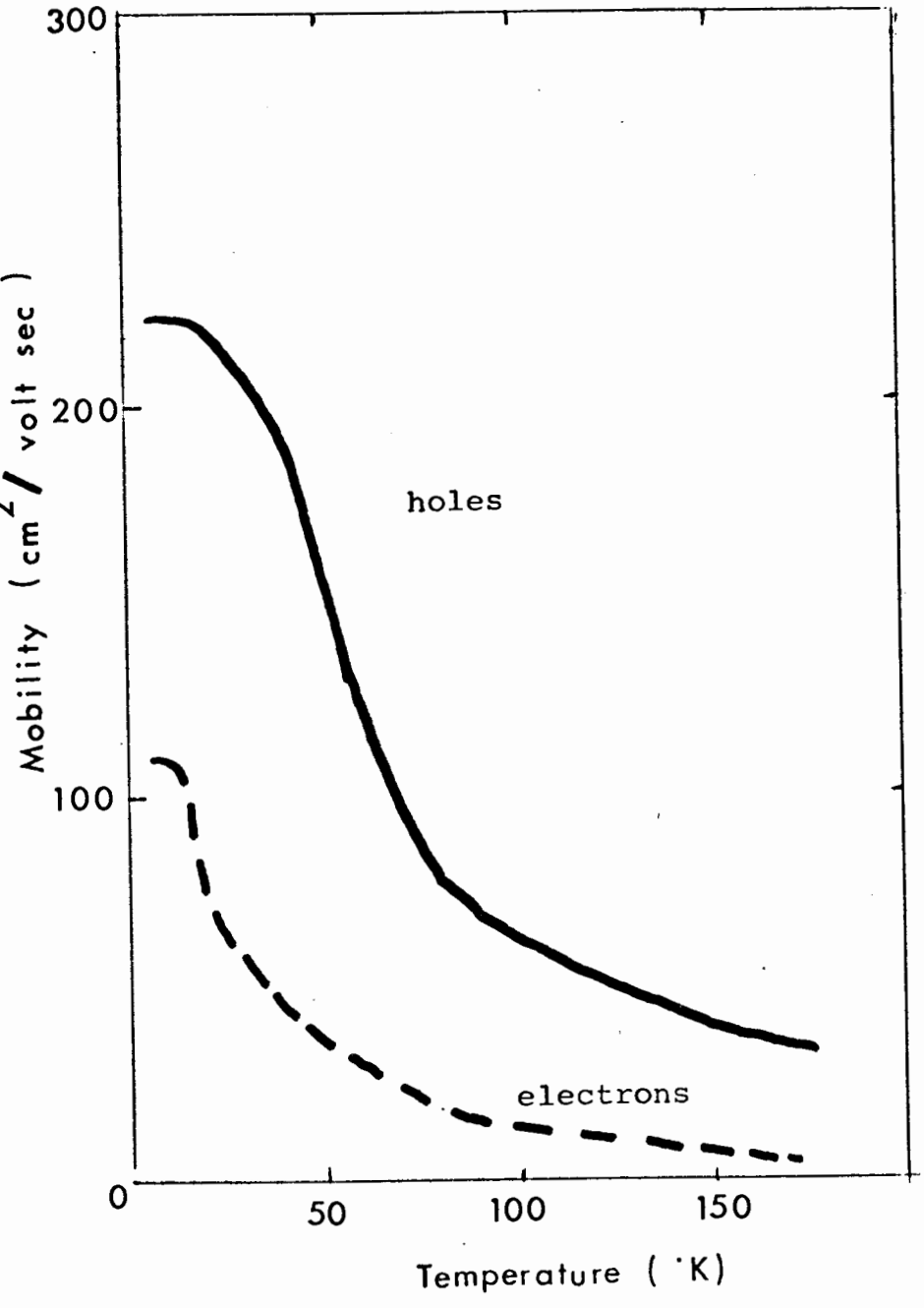

Fig. 5.2 Mobility-temperature curve for $NbSe_2$, calculated on the basis of $n_e = 10n_h$.

and $n_h = 0.5 \times 10^{21}/cm^3$. (This compares with 1.5×10^{21} Nb atoms/cm^3). The conductivity is dominated by the large number of low mobility electrons at all temperatures, but at high temperatures the Hall effect is dominated by the high mobility holes, notwithstanding their low density.

The two-band model presented here provides a reasonable explanation for the observed reversal in the Hall coefficient. Other explanations offered require phase changes to occur, and it is likely that a phase change would cause discontinuities in the resistivity and Hall coefficient, rather than the continuous variations observed in practice.

5.3 Nuclear magnetic resonance experiments

The observed value of the quadrupole coupling constant at 77°K (61.68 ± 0.05 MHz) agrees with the result of Geballe et al (1971) on $NbSe_2$ powder (61.4 ± 0.3 MHz) at the same temperature. At 17.7°K the linewidth of the main 1/2 - -1/2 transition increased such that the satellite lines were not visible. As a result it was not possible to test the hypothesis of Geballe et al (1971) that the two Nb sites in the unit cell had different quadrupole coupling constants at 4.2°K and that the axial symmetry of the Nb^{93} nucleus observed at 77°K was not present at 4.2°K.

A metal such as Nb, at 77°K, will have a linewidth of the

order of 4 gauss, and at $4^{o}K$ the linewidth will be about 2 gauss. Lowering the temperature to $4^{o}K$ approximately halves the linewidth. However in the case of $NbSe_2$ the linewidth increases by a factor of 3 on cooling from $77^{o}K$ to $17.7^{o}K$.

Now the linewidth of an NMR signal in a metal is dependent on the defects in the sample, and also on the hyperfine coupling between nuclear and conduction electron spins. The defect linewidth is independent of temperature, while that of the spin-spin coupling depends linearly on temperature, as will be shown below.

The hyperfine coupling between the nuclear spins and the conduction electrons produces a modification of the energy levels of the nuclear spin system. This is observed as the Knight shift (Townes 1950). This same hyperfine coupling serves as the main mechanism for spin-lattice relaxation in metals. The resulting linewidth ΔH_L is proportional to the reciprocal of the spin-lattice relaxation time T_1

$$\Delta H_L \alpha \frac{1}{T_1} \qquad (5.12)$$

An order of magnitude estimate of $\frac{1}{T}$ is given by Abragam (1961, p. 357). The probability of a spin-flip is the product of three terms:

(i) only a fraction $\frac{kT}{E_F}$ of the conduction electrons can take up the small energy associated with a spin-flip.

(ii) a conduction electron can only be localised on a particular nucleus for a time $\tau_c \sim \frac{\hbar}{E_F}$ by uncertainty principle arguments.

(iii) the hyperfine interaction $H_1 = \frac{8\pi}{3}\hbar\gamma_e\gamma_n\,\delta(r_I)\,\underline{I}.\underline{S}$ is responsible for the spin-flips.

Then the transition probability for a spin-flip $\frac{kT}{E_F}|H_1|^2\tau_c$

$$\frac{1}{T} \sim \frac{kT}{E_F}\,\frac{\hbar}{E_F}\left(\frac{8\pi}{3}\right)^2\gamma_n{}^2\gamma_e{}^2\hbar^2\,|\psi(0)|^4$$

$$\frac{1}{T_1} \sim \left(\frac{8\pi}{3}\right)^2\gamma_e{}^2\gamma_n{}^2\hbar^2\,|\psi(0)|^4\,\frac{kT}{E_F{}^2} \qquad (5.13)$$

where γ_e, γ_n are gyromagnetic ratios of electron and nucleus, and ψ is the electronic wavefuction for a conduction electron. Thus the linewidth is proportional to temperature and to the fourth power of the electronic wavefunction $\psi(0)$ of the conduction electrons at the Nb^{93} nucleus. The results obtained in this work suggest that changes in the band structure of $NbSe_2$ occur below $77^{\circ}K$. From his results Geballe (1971) suggests that there is a redistribution of the electrons within the unit cell, and he suggests that the p-to-n transition may be connected in some way with this redistribution. Unfortunately this work does not go far enough to be able to comment on this hypothesis.

5.4 Suggestions for further work

On the experimental side, there are three possible lines

of attack. The first would be to find some iron-free $NbSe_2$, either by the purchase of iron-free niobium* or by chemical separation of the iron from the niobium. Chlorine gas has been used successfully (Walker 1970) to separate iron from gold, and the use of a halogen may accomplish the same with niobium. Purer $NbSe_2$ would make de-Haas - Van Alphen measurements possible. So far these have failed (Wilson and Yoffe 1969) but larger purer crystals may make it possible to determine the Fermi surface of $NbSe_2$.

Optical transmission and reflection spectra, both off faces and off edges, can be carried out at high ($77^{o}K$) and low ($7^{o}K$) temperatures and the results compared to see if there are any changes in the band structure in the intervening temperature interval.

A change in lattice parameters can be detected by monitoring the thermal expansion coefficient as a function of temperature. It may be possible to estimate the sharpness of the change in lattice parameters previously reported.

Development of more sensitive broad-line NMR spectrometers will enable the fine structure of the Nb nucleus to be explored.

---

* A survey of the major suppliers of niobium powder shows that the minimum iron content in high grade niobium is of the order of 50 parts per million.

Powder NMR results are difficult to interpret, and the more direct single crystal methods can be used to give clear indications of any structural or electronic phase changes that may occur in $NbSe_2$ in the temperature range from $7^{o}K$ to $77^{o}K$.

On the theoretical side, models of the Fermi surface, band structure and phonon spectrum are needed, so that predictions of such properties as magnetoresistance, electrical conductivity, lattice specific heat etc., can be made. Testing against existing experimental data would serve to refine the theoretical descriptions of $NbSe_2$ and other related layer structures.

Appendix A: NMR energy levels for the case of the magnetic field not parallel to the c-axis in $NbSe_2$

In section 4.2 an exact solution of the Schrodinger equation was possible as the Zeeman and quadrupolar parts of the Hamiltonian operated on the same set of wavefunctions. When the magnetic field is not aligned along the symmetry axis of the nucleus, this is no longer true, and a perturbation approach is used instead. (An exact solution is possible by simultaneously diagonalising both parts of the Hamiltonian, but this requires a considerable labour in inverting the matrices.)

Let the magnetic field be along the z' axis, and the weak quadrupolar interaction be along the z axis, at an angle θ with the z' axis.

$$H = -\gamma_r \hbar H_0 I_{z'} + \frac{e^2 q Q}{4I(2I-1)} \left[3I_z^2 - I^2 \right] \tag{A.1}$$

Now
$$\begin{aligned} I_z &= I_{z'} \cos\theta + I_{x'} \sin\theta \\ I_x &= I_{x'} \cos\theta - I_{z'} \sin\theta \\ I_y &= I_{y'} \end{aligned} \tag{A.2}$$

Putting the transformation (A.2) into (A.1)

$$\begin{aligned} H = -\gamma_r \hbar H_0 I_{z'} + \frac{e^2 q Q}{4I(2I-1)} \Big[& 3I_{z'}^2 \cos^2\theta \\ & + 3\sin\theta\cos\theta (I_{z'} I_{x'} + I_{x'} I_{z'}) \\ & + 3I_{x'}^2 \sin^2\theta - I^2 \Big] \end{aligned} \tag{A.3}$$

To simplify (A.3) use first order terms only.

Then $I_{z'}$ is diagonal

$I_{x'}$ has no diagonal elements

Therefore $I_{z'}\, I_{x'} \left| m \right> = 0$

$$E_m = \left< m \right| H \left| m \right>$$

$$= -\gamma_n \hbar H_0 m + \frac{e^2 q Q}{4I(2I-1)} \left[3\cos^2\theta \left< m \right| I_{z'}^2 \left| m \right> + 3\sin^2\theta \left< m \right| I_{x'}^2 \left| m \right> - \left< m \right| I^2 \left| m \right> \right] \qquad (A.4)$$

(A.4) after a little algebra becomes

$$E_m = -\gamma_n \hbar H_0 m + \frac{e^2 q Q}{4I(2I-1)} \left[\frac{3\cos^2\theta - I}{2} \right] \left[3m^2 - I(I+1) \right] \qquad (A.5)$$

(A.5) gives the energy levels in this case.

For the 3/2 - 1/2 transition

$$\Delta E_{\frac{3}{2}-\frac{1}{2}} = -\gamma_n \hbar H_0 + \frac{3e^2 q Q}{4I(2I-1)} \left[3\cos^2\theta - 1 \right] \qquad (A.6)$$

The 3/2 - 1/2 transition frequency is a minimum when $3\cos^2\theta - 1$ is a maximum, i.e., when $\theta = 0°$ or when the magnetic field is aligned parallel to the c-axis. This justifies the final

orientation procedure used in the NMR experiments.

Second order perturbation theory shows that the 1/2 - -1/2 transition also has a minimum transition frequency when $\theta = 0^{\circ}$, so orientation is also possible using the main Nb^{93} line. The proof is non-trivial and will be omitted.

REFERENCES

A. Abragam, The principles of nuclear magnetism , Oxford University Press, (1961) .

A. Antonova, C.A. Medeev, I.Yu. Shebalin, Zh. Eks. Teor. Fiz. 57 , 329 (1969) . [English translation , Soviet Physics JETP, 30 , 181 (1970)]

J. Bardeen, L.N. Cooper, J.R.Schrieffer, Phys. Rev. 108, 1175 (1957) .

R. Berman, J.C.F. Brock, D.J.Huntley, Cryogenics 4 , 233 (1964)

G. Borelius, W.H. Keesom, C.H. Johanssen, J.O. Linde, Proc. Kon. Akad. Amsterdam 35 , 10 (1932) .

L.H. Brixner, J. Inorg. Chem. 24 , 257 (1962).

B.E. Brown, D.J. Beerntsen, Acta Cryst. 18 , 31 (1965).

A.C. Chapman, P. Rhodes, E.F.W. Seymour, Proc. Phys. Soc. 70B , 345 (1957) .

B. Clayman, R.F. Frindt, submitted to Phys. Rev. Letters (1971) .

R.W. Cohen, E.D. Cody, J.J. Halloran, Phys. Rev. Letters 19 , 840 (1967) .

W.J. de Sorbo, W.W. Tyler, J. Chem. Phys. 21, 1660 (1953) .

W.J. de Sorbo, G.E. Nichols, J. Phys. Chem. Solids 6 , 352 (1958) .

R.F. Frindt, J. appl. Phys. 37 , 1928 (1966) .

T.H. Geballe, E. Ehrenfreund, F.R. Gamble, A.C. Gossard, J. appl. Phys. 42 , 1491 (1971) .

J.B. Goodenough, Mat. Res. Bull. 3 , 409 (1968) .

F. Hulliger, in Structure and bonding, vol. 4, ed. C. Jorgenson, Springer Verlag, Berlin (1968) .

D.J. Huntley, unpublished work, S.F.U. (1971) .

R. Kershaw, M. Vlasse, A. Wold, Inorg. Chem. 6 , 1599 (1965) .

C. Kittel, Introduction to solid state physics , Wiley, New York, (1966) .

J. Kopp, D.Phil. thesis, Oxford University. (1969)

J.A. Krumhansl, H. Brooks, J.Chem. Phys. 21, 1663 (1953) .

H.N.S. Lee, H. McKinzie, D.S. Tannhauser, A. Wold, J. appl. Phys. 40 , 602 (1969) .

H.N.S. Lee, H. McKinzie, A. Wold, J. Solid State Chem. 1, 190 (1970).

G.T. Meaden, Electrical resistance in metals , Plenum Press, New York (1965) .

G.F. Newell, J. Chem. Phys. 23 , 2431 (1955) .

J.F. Nye, Physical properties of crystals, Oxford University Press, (1957) .

R.V. Pound, W.D. Knight, Rev. Sci. Inst. 21 , 219 (1950) .

W. Primak, L.H. Fuchs, Phys. Rev. 95 , 22 (1954) .

E. Revolinsky, C.H. Armitage, D.J. Beerntsen, B.E. Brown, J. less common metals 8 , 63 (1965) ,

H. Schafer, Chemical transport reactions , Academic Press, New York (1964) .

K. Selte, A. Kjekshus, Acta. chem. scand. 19 ,258 (1965) .

S. Sharma, Ph.D. thesis, University of British Columbia (1967) .

R.E. Sherriff, D. Williams, Phys. Rev. 82 , 651 (1951) .

C. Slichter, Principles of magnetic resonance , Harper, Row, New York, (1963) .

H.H. Soonpaa, J. appl. Phys. 33 , 2542 (1962) .

C.H. Townes, C. Herring, W.D. Knight, Phys. Rev. 77 , 852 (1950).

L.J. van der Pauw, Phillips Techn. Reports, 16 , 187 (1961) .

M.H. van Maaren, H.B. Harland, Phys. Letters 29A , 571 (1969) .

C.W.E. Walker, Can. J. Phys. 48 , 378 (1970) .

A.H. Wilson, Theory of metals , Cambridge University Press (1953) .

J.A. Wilson, A.D. Yoffe, Advances in Physics 18 , 193 (1969) .

A. Wold, private communication, (1971) .